Article

Directed Assembly of Transition-Metal-Coordinated Molecular Loops and Squares from Salen-Type Components. Examples of Metalation-Controlled Structural Conversion

Shih-Sheng Sun, Charlotte L. Stern, SonBinh T. Nguyen, and Joseph T. Hupp

J. Am. Chem. Soc., **2004**, 126 (20), 6314-6326• DOI: 10.1021/ja037378s • Publication Date (Web): 30 April 2004

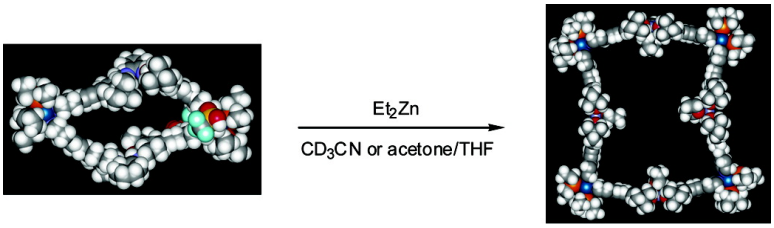

More About This Article

Additional resources and features associated with this article are available within the HTML version:

- Supporting Information
- Links to the 13 articles that cite this article, as of the time of this article download
- Access to high resolution figures
- Links to articles and content related to this article
- Copyright permission to reproduce figures and/or text from this article

View the Full Text HTML

J|A|C|S
ARTICLES
Published on Web 04/30/2004

Directed Assembly of Transition-Metal-Coordinated Molecular Loops and Squares from Salen-Type Components. Examples of Metalation-Controlled Structural Conversion

Shih-Sheng Sun, Charlotte L. Stern, SonBinh T. Nguyen,* and Joseph T. Hupp*

Contribution from the Department of Chemistry, Center for Nanofabrication and Molecular Self-Assembly, and Institute for Environmental Catalysis, Northwestern University, 2145 Sheridan Road, Evanston, Illinois 60208

Received July 18, 2003; E-mail: stn@northwestern.edu; j-hupp@northwestern.edu

Abstract: A series of transition-metal-containing molecular "loops" and "squares" has been prepared via a directed-assembly approach and characterized. The molecular loops were prepared from the reaction of *cis*-$(PEt_3)_2Pt(OTf)_2$ with bis(4-pyridyl)-functionalized free-base salen-type ligands. Zn(II)-metalation of the salen-type ligands in the molecular loops converts the loops to molecular squares. Alternatively, the squares can be obtained by the directed assembly of *cis*-$(PEt_3)_2Pt(OTf)_2$ and bis(4-pyridyl)-functionalized Zn(II)−salen-type ligands. A concentration-dependent dynamic equilibrium between cyclic species was observed when bis(3-pyridyl)-functionalized free-base salen-type ligand was employed in the reaction. Zn(II) or Cr(III) metalation of the free-base ligand shifted the equilibrium to the single dimeric species. The incorporation of multiple reactive metal sites into a single, cavity-containing supramolecular structure points toward catalytic applications for these new assemblies.

Introduction

The use of weak coordination interactions to construct large macrocyclic structures under thermodynamic control has attracted enormous attention in the past decade.[1] By judicious design of preprogrammed synthons, the desired supramolecular structures can usually be obtained in a single step; in other words, synthesis can be accomplished via "directed assembly". For example, a simple square structure can be prepared from four transition-metal components, each with two available cis positions, and four rigid or semirigid bifunctional ligands. However, the potential number of structural variations tends to increase with increasing flexibility of the ligands. For example, equilibria between molecular triangles and squares have been documented in systems employing flexible linkers.[2] The not uncommon observation of preferential formation of a smaller cyclic structure over a larger structure in the absence of proper templates indicates that entropy maximization can be a dominant effect in these directed-assembly processes.[3,4]

We have recently developed a series of bifunctional salen-type[5] ligands to serve as building blocks for cyclic supramolecular structures.[6,7] Metallosalen complexes are of considerable current interest due to their ubiquitous use in a variety of catalytic chemical transformations. Examples where salen complexes offer both high reactivity and selectivity include epoxidation of olefins, asymmetric ring-opening of epoxides, olefin aziridination, olefin cyclopropanation, and formation of cyclic and linear polycarbonates.[8] It has been well-documented in recent reports that the mechanisms of several of the aforementioned catalytic chemical transformations proceed through cooperative bimetallic processes.[9] For these reactions, molecular systems containing two or more reactive metal centers capable of cooperative interactions are promising candidates for the development of highly efficient catalytic materials.

Recently, we and others have shown that supramolecular compounds incorporating multiple active sites can be easily

(1) (a) Leininger, S.; Olenyuk, B.; Stang, P. J. *Chem. Rev.* **2000**, *100*, 853−907. (b) Holliday, B. J.; Mirkin, C. A. *Angew. Chem., Int. Ed.* **2001**, *40*, 2022−2043. (c) Dinolfo, P. H.; Hupp, J. T. *Chem. Mater.* **2001**, *13*, 3113−3125. (d) Caulder, D. L.; Raymond, K. N. *J. Chem. Soc., Dalton Trans.* **1999**, 1185−1120.

(2) (a) Schweiger, M.; Seidel, S. R.; Arif, A. M.; Stang, P. J. *Inorg. Chem.* **2002**, *41*, 2556−2559. (b) Sautter, A.; Schmid, D. G.; Jung, G.; Würthner, F. *J. Am. Chem. Soc.* **2001**, *123*, 5424−5430. (c) Cotton, F. A.; Daniels, L. M.; Lin, C.; Murillo, C. A. *J. Am. Chem. Soc.* **1999**, *121*, 4538−4539. (d) Lee, S. B.; Hwang, S.; Chung, D. S.; Yun, H.; Hong, J.-I. *Tetrahedron Lett.* **1998**, *39*, 873−876. (e) Fujita, M.; Sasaki, O.; Mitsuhashi, T.; Fujita, T.; Yazaki, J.; Yamaguchi, K.; Ogura, K. *Chem. Commun.* **1996**, 1535−1536. (f) Schnebeck, R.-D.; Freisinger, E.; Lippert, B. *Eur. J. Org. Chem.* **2000**, 1193−1200. (g) Park, K.-M.; Kim, S.-Y.; Heo, J.; Whang, D.; Sakamoto, S.; Yamaguchi, K.; Kim, K. *J. Am. Chem. Soc.* **2002**, *124*, 2140−2147.

(3) (a) Kuehl, C. J.; Huang, S.; Stang, P. J. *J. Am. Chem. Soc.* **2001**, *123*, 9634−9641. (b) Sun, S.-S.; Lees, A. J. *J. Am. Chem. Soc.* **2000**, *122*, 8956−8967. (c) Slone, R. V.; Benkstein, K. D.; Bélanger, S.; Hupp, J. T.; Guzei, I. A.; Rheingold, A. L. *Coord. Chem. Rev.* **1998**, *171*, 221−243. (d) Slone, R. V.; Yoon, D. I.; Calhoun, R. M.; Hupp, J. T. *J. Am. Chem. Soc.* **1995**, *117*, 11813−11814. (e) Sun, S.-S.; Lees, A. J. *Coord. Chem. Rev.* **2002**, *230*, 171−192.

(4) We note, however, that there are examples where the formation of the smaller assembly is enthalpically driven due to solvation effects. See: (a) Bark, T.; Düggeli, M.; Stoeckli-Evans, H.; von Zelewsky, A. *Angew. Chem., Int. Ed.* **2001**, *40*, 2848−2851. (b) Mamula, O.; Monlien, F. J.; Porquet, A.; Hopfgartner, G.; Merbach, A. E.; von Zelewsky, A. *Chem. Eur. J.* **2001**, *7*, 533−539.

(5) For the remainder of this article, the term *salen* will be used to describe the general class of bis(salicylaldimine) ligands and complexes.

(6) Morris, G. A.; Zhou, H.; Stern, C. L.; Nguyen, S. T. *Inorg. Chem.* **2001**, *40*, 3222−3227.

(7) Splan, K. E.; Massari, A. M.; Morris, G. A.; Sun, S.-S.; Reina, E.; Nguyen, S. T.; Hupp, J. T. *Eur. J. Inorg.* **2003**, 2348−2351.

(8) Canali, L.; Sherrington, D. C. *Chem. Soc. Rev.* **1999**, *28*, 85−93.

(9) (a) Hansen, K. B.; Leighton, J. L.; Jacobsen, E. N. *J. Am. Chem. Soc.* **1996**, *118*, 10924−10925. (b) Tokunaga, M.; Larrow, J. F.; Kakiuchi, F.; Jacobsen, E. N. *Science* **1997**, *277*, 936−938. (c) Paddock, R. L.; Nguyen, S. T. *J. Am. Chem. Soc.* **2001**, *123*, 11498−11499.

10.1021/ja037378s CCC: $27.50

synthesized in high yield via directed-assembly strategies.[10] In addition, several groups, including ours, have already utilized reactive supramolecular structures to initiate or enhance catalytic processes.[11,12] Much of our own current effort is directed toward the construction of supramolecular systems that are capable of performing a variety of catalytic chemical transformations. In this paper, we wish to report the preparation of a series of dinuclear molecular loops and molecular squares incorporating salen-type ligands—noting that salen-type structures comprise essential ligand frameworks for several transition-metal-based catalysts. We find that free-base salen-linked molecular loops can be quantitatively converted to molecular squares by reducing the flexibility of the ligand via Zn(II) metalation. To the best of our knowledge, in the absence of template effects quantitative conversions of this kind (i.e., supramolecular rearrangements accompanying changes in metal nuclearity) are unprecedented. Finally, we have also observed a concentration-dependent dynamic equilibrium between mono-, di-, and trinuclear Pt(II) complexes constructed from related free-base 3,3′-dipyridyl salen ligands. Quantitative conversion to the cyclic dinuclear complex can be effected by rigidifying the salen framework via Zn(II) or Cr(III) incorporation.

Experimental Section

Materials and General Procedures. The starting materials, *cis*-$(PEt_3)_2Pt(OTf)_2$,[13] 4-ethynylpyridine,[14] 5-bromo-3-*tert*-butyl-2-hydroxybenzaldehyde,[15] 3-*tert*-butyl-2-hydroxy-5-(3-pyridinyl)benzaldehyde,[16] Schiff base ligands (**1**, **2**, and **3**),[6] and Zn salen ligands (**Zn-1**, **Zn-2**, and **Zn-3**)[6] were prepared according to published methods. Dichloromethane was distilled over calcium hydride. Tetrahydrofuran (THF) and diethyl ether were distilled over sodium/benzophenone. All solvents were distilled under nitrogen and saturated with nitrogen prior to use. Deuterated solvents were purchased from Cambridge Isotope Laboratories and used without further purification. All other chemical reagents were commercially available from either Aldrich or Lancaster Synthesis and used without further purification unless otherwise noted.

All reactions and manipulations were carried out under inert nitrogen atmosphere with the use of standard Schlenk techniques. Flash column chromatography was carried out with 230−400 mesh silica gel from Aldrich using the wet-packing method. NMR spectra were recorded on either a Mercury 400 (400.168 MHz for ^{1}H, 100.622 MHz for ^{13}C, 161.991 MHz for ^{31}P, and 376.534 MHz for ^{19}F) or an Inova 500 (499.773 MHz for ^{1}H, 125.669 MHz for ^{13}C) spectrometer. ^{1}H NMR data are reported as follows: chemical shift (multiplicity (b = broad, s = singlet, d = doublet, t = triplet, q = quartet, and m = multiplet), and integration). ^{1}H and ^{13}C chemical shifts are reported in parts per million downfield from tetramethylsilane (TMS, δ scale) with the solvent resonances as internal standards. ^{31}P NMR spectra are reported in parts per million relative to external 85% H_3PO_4 at 0.00 ppm, and ^{19}F NMR spectra are reported in parts per million relative to external $CFCl_3$ at 0.00 ppm. Elemental analysis was performed by Oneida Research Service (Whitesboro, NY). Electrospray mass spectra (ESIMS) were obtained in the Analytical Services Laboratory at Northwestern University using a Micromass Quatro II mass spectrometer equipped with an electrospray interface.

3-*tert*-Butyl-5-(4′-ethynylpyridyl)-2-hydroxybenzaldehyde. Under nitrogen, a 200-mL Schlenk flask equipped with a magnetic stirbar and a reflux condenser was charged with 4-ethynylpyridine (0.60 g, 5.8 mmol), 5-bromo-3-*tert*-butyl-2-hydroxybenzaldehyde (1.0 g, 3.9 mmol), $Pd(PPh_3)_4$ (150 mg, 0.13 mmol), CuI (25 mg, 0.13 mmol), and ^{i}Pr$_2$NH (100 mL) and refluxed for 18 h. After the reaction, the volatile solvent was removed under reduced pressure. Subsequently, water (100 mL) was added and the brown suspension was extracted with diethyl ether (3 × 100 mL). The organic layer was collected, dried over Na_2SO_4, filtered through a short neutral alumina column, and then evaporated to dryness. The resulting brown residue was dissolved in CH_2Cl_2 and loaded on silica gel (5 cm × 20 cm) and subjected to column chromatography with CH_2Cl_2/MeOH (99/1) eluent. The desired product eluted as a yellow band which was collected and evaporated on a rotary evaporator to yield a yellow solid (0.67 g, 62%). ^{1}H NMR (400 MHz, $CDCl_3$): δ 12.0 (s, 1 H), 9.90 (s, 1 H), 8.62 (d, 2 H, J = 6.0 Hz), 7.68 (s, 1 H), 7.67 (s, 1 H), 7.39 (d, 2 H, J = 6.0 Hz), 1.45 (s, 9 H). ^{13}C NMR (100 MHz, $CDCl_3$): δ 161.9, 149.8, 139.3, 137.2, 135.7, 131.4, 125.5, 120.6, 113.2, 94.5, 93.2, 85.9, 35.3, 29.4. Anal. Calcd for $C_{18}H_{17}NO_2$: C, 77.40; H, 6.13; N, 5.01. Found: C, 76.96; H, 6.14; N, 4.64.

3-*tert*-Butyl-5-(3′-ethynylpyridyl)-2-hydroxybenzaldehyde. Essentially the same procedure as above was employed to synthesize this compound. The desired product was eluted as a yellow band with CH_2Cl_2/NEt_3 mixture (99/1), and the solvent was then evaporated to give a yellowish solid (57%). This material is adequately pure to use for next synthesis without further purification. ^{1}H NMR (400 MHz, $CDCl_3$): δ 12.0 (s, 1 H), 9.89 (s, 1 H), 8.77 (s, 1 H), 8.56 (d, 1 H, J = 4.8 Hz), 7.81 (d, 1 H, J = 6.4 Hz), 7.68 (s, 1 H), 7.65 (s, 1 H), 7.30 (m, 1 H), 1.45 (s, 9 H).

General Procedure for the Synthesis of Ligands 4−8. A mixture of the corresponding aldehyde (4 mmol), diamine (2 mmol), and EtOH (40 mL) was refluxed in a 100-mL round-bottom flask equipped with a magnetic stirbar and a water-cooled reflux condenser for 16 h. If the product precipitated out from solution, it was isolated by filtration, washed with EtOH (5 mL), and dried in vacuo. If the product was soluble in EtOH, water was added until the solution became cloudy. After storage of this mixture for 10 h in a freezer (−10 °C), the precipitate was collected on a frit, washed with cold EtOH (5 mL), and dried in vacuo.

1,2-Diaminobenzene-*N*,*N*′-bis(3-*tert*-butyl-5-(3′-pyridyl)salicylidene) (4). This compound was isolated as an orange-red solid (42%). ^{1}H NMR (400 MHz, DMSO-d_6): δ 14.2 (s, 2 H), 9.11 (s, 2 H), 8.89 (s, 2 H), 8.54 (d, 2 H, J = 4.8 Hz), 8.06 (d, 2 H, J = 7.6 Hz), 7.93 (s, 2 H), 7.66 (s, 2 H), 7.58 (dd, 2 H, J = 6.4 Hz), 7.50−7.47 (m, 4 H), 1.45 (s, 18 H). Anal. Calcd for $C_{38}H_{38}N_4O_2$: C, 78.32; H, 6.57; N, 9.61. Found: C, 78.16; H, 6.69; N, 9.46.

***meso*-1,2-Diaminocyclohexane-*N*,*N*′-bis(3-*tert*-butyl-5-(3′-pyridyl)-salicylidene) (5).** The isolated precipitate from ethanol solution was subjected to column chromatography on silica gel eluted with ethyl acetate/hexane (4/1) to yield a yellow band containing the meso isomer which was collected and evaporated on a rotary evaporator to give a yellow solid (34%). ^{1}H NMR (400 MHz, $CDCl_3$): δ 14.1 (s, 2 H), 8.70 (d, 2 H, J = 2.4 Hz), 8.52 (d, 2 H, J = 3.6 Hz), 8.37 (s, 2 H), 7.71 (d, 2 H, J = 8.0 Hz), 7.44 (d, 2 H, J = 2.0 Hz), 7.30 (dd, 2 H, J = 8.4 Hz), 7.19 (d, 2 H, J = 2.0 Hz), 3.40 (m, 2 H), 2.07−1.80 (m, 8 H), 1.44 (s, 18 H). ^{13}C NMR (100 MHz, $CDCl_3$): δ 165.5, 160.6, 147.9, 147.8, 138.2, 136.5, 133.8, 128.3, 128.2, 127.4, 123.5, 118.9, 72.6,

(10) (a) Hupp, J. T.; Nguyen, S. T. *Electrochem. Soc. Interface* **2001**, *10* (3), 28−32. (b) Anderson, S.; Anderson, H. L.; Sanders, J. K. M. *Acc. Chem. Res.* **1993**, *26*, 469−475.
(11) (a) Fujita, M.; Kwon, Y. J.; Washizu, S.; Ogura, K. *J. Am. Chem. Soc.* **1994**, *116*, 1151−1152. (b) Kang, J.; Rebek, J., Jr. *Nature* **1997**, *385*, 50−52. (c) Ooi, T.; Kondo, Y.; Maruoka, K. *Angew. Chem., Int. Ed.* **1998**, *37*, 3039−3041. (d) Nakash, M.; Clyde-Watson, Z.; Feeder, N.; Davies, J. E.; Teat, S. J.; Sanders, J. K. M. *J. Am. Chem. Soc.* **2000**, *122*, 5286−5293. (e) Seo, J. S.; Whang, D.; Lee, H.; Jun, S. I.; Oh, J.; Jeon, Y. J.; Kim, K. *Nature* **2000**, *404*, 982−986.
(12) (a) Merlau, M. L.; del Pilar Mejia, M.; Nguyen, S. T.; Hupp, J. T. *Angew. Chem., Int. Ed.* **2001**, *40*, 4239−4242. (b) Morris, G. A.; Nguyen, S. T.; Hupp, J. T. *J. Mol. Catal. A: Chem.* **2001**, *174*, 15−20. (c) Merlau, M. L.; Grande, W. J.; Nguyen, S. T.; Hupp, J. T. *J. Mol. Catal. A: Chem.* **2000**, *156*, 79−84.
(13) Stang, P. J.; Cao, D. H.; Saito, S.; Arif, A. M. *J. Am. Chem. Soc.* **1995**, *117*, 6273−6283.
(14) Whiteford, J. A.; Lu, G. V.; Stang, P. J. *J. Am. Chem. Soc.* **1997**, *119*, 2524−2533.
(15) Larrow, J. F.; Jacobsen, E. N.; Gao, Y.; Hong, Y.; Nie, X.; Zepp, C. M. *J. Org. Chem.* **1994**, *59*, 1939−1942.
(16) Morris, G. A.; Nguyen, S. T. *Tetrahedron Lett.* **2001**, *42*, 2093−2096.

35.3, 33.6, 29.6, 24.6. EIMS: found *m*/*z* 588.5, calcd *m*/*z* 588.3 (M^+). Anal. Calcd for $C_{38}H_{44}N_4O_2 \cdot 0.5C_4H_8O_2$: C, 75.92; H, 7.65; N, 8.85. Found: C, 76.26; H, 7.23; N, 9.13.

***rac*-1,2-Diaminocyclohexane-*N,N′*-bis(3,5-di-*tert*-butyl-5-(3-pyridyl)-salicylidene) (6).** The isolated precipitate from ethanol solution was subjected to column chromatography on silica gel eluted with ethyl acetate/^{i}Pr$_2$NH (99/1) to yield a yellow band containing the rac isomer which was collected and evaporated on a rotary evaporator to give a yellow solid (54%). ^{1}H NMR (100 MHz, $CDCl_3$): δ 14.2 (s, 2 H), 14.1 (s, 2 H), 8.81 (s, 2 H), 8.70 (s, 2 H), 8.55 (d, 2 H, J = 3.6 Hz), 8.51 (s, 4 H), 8.36 (s, 2 H), 7.82 (d, 2 H, J = 7.2 Hz), 7.71 (d, 2 H, J = 7.2 Hz), 7.54 (s, 2 H), 7.43 (s, 2 H), 7.34 (bs, 4 H), 7.29 (m, 2 H), 7.19 (s, 2 H), 3.38 (m, 4 H), 2.05−1.67 (m, 16 H), 1.49 (s, 18 H), 1.43 (s, 18 H). ^{13}C NMR (100 MHz, $CDCl_3$): δ 165.4, 164.9, 160.7, 160.5, 147.9, 147.82, 147.76, 147.71, 138.4, 138.1, 136.5, 136.4, 133.8, 133.7, 128.3, 128.24, 128.16, 128.1, 127.41, 127.36, 123.5, 123.4, 118.9, 118.8, 76.7, 72.5, 35.3, 35.2, 33.9, 33.6, 29.6, 29.5, 25.2, 24.9. APCIMS: found *m*/*z* 589.48, calcd *m*/*z* 589.35 for [MH^+]. Anal. Calcd for $C_{38}H_{44}N_4O_2 \cdot C_4H_8O_2 \cdot H_2O$: C, 72.59; H, 7.83; N, 8.06. Found: C, 72.36; H, 7.79; N, 8.12.

1,2-Diaminobenzene-*N,N′*-bis(3-*tert*-butyl-5-(4′-ethynylpyridyl)-salicylidene) (7). This compound was isolated as a red solid (88%). ^{1}H NMR (400 MHz, $CDCl_3$): δ 14.2 (s, 2 H), 8.68 (s, 2 H), 8.60 (d, 4 H, J = 5.2 Hz), 7.57 (s, 2 H), 7.53 (s, 2 H), 7.41 (m, 2 H), 7.38 (d, 4 H, J = 5.2 Hz), 7.30 (m, 2 H), 1.46 (s, 18 H). ^{13}C NMR ($CDCl_3$): δ 163.4, 161.9, 149.7, 142.0, 138.9, 134.6, 134.1, 131.9, 128.2, 125.5, 119.8, 119.2, 111.9, 94.5, 85.4, 35.4, 29.5. ESIMS: found *m*/*z* 631.2, calcd *m*/*z* 631.3 for [MH^+]. Anal. Calcd for $C_{42}H_{38}N_4O_2 \cdot C_2H_5OH$: C, 78.08; H, 6.55; N, 8.28. Found: C, 77.99; H, 6.20; N, 8.23. Single crystals of **7**·CH_2Cl_2 were obtained by slow evaporation from a CH_2Cl_2/hexane mixture.

1,2-Diaminobenzene-*N,N′*-bis(3-*tert*-butyl-5-(3′-ethynylpyridyl)-salicylidene) (8). This compound was isolated as a red solid (54%). ^{1}H NMR ($CDCl_3$): δ 14.1 (s, 2 H), 8.77 (s, 2 H), 8.68 (s, 2 H), 8.54 (d, 2 H, J = 5.2 Hz), 7.81 (d, 2 H, J = 8.0 Hz), 7.57 (s, 2 H), 7.51 (d, 2 H, J = 1.6 Hz), 7.40 (m, 2 H), 7.30 (m, 4 H), 1.46 (s, 18 H). ^{13}C NMR (400 MHz, $CDCl_3$): δ 163.5, 161.6, 152.2, 148.3, 142.0, 138.8, 138.3, 134.2, 133.9, 128.2, 123.1, 120.8, 119.8, 119.2, 112.3, 92.9, 84.5, 35.4, 29.5. ESIMS: found *m*/*z* 631.2, calcd *m*/*z* 631.3 for (MH^+). Anal. Calcd for $C_{42}H_{38}N_4O_2 \cdot 2H_2O$: C, 75.65; H, 6.35; N, 8.40. Found: C, 75.49; H, 6.55; N, 8.28.

General Procedure for the Synthesis of Ligands Zn-7 and Zn-8. In a drybox, Et_2Zn (0.5 mmol) was added to a 50-mL round-bottom flask containing a stirred solution of appropriate Schiff base ligand (0.5 mmol) in THF (10 mL) at room temperature, and the mixture was stirred for 16 h. The precipitate was collected on a frit, washed with cold THF (5 mL), and dried under reduced pressure.

1,2-Diaminobenzene-*N,N′*-bis(3-*tert*-butyl-5-(4′-ethynylpyridyl)-salicylidene)zinc(II)·THF (Zn-7). This compound was isolated as an orange solid (99%). ^{1}H NMR (DMSO-d_6): δ 9.11 (s, 2 H), 8.57 (d, 4 H, J = 4.4 Hz), 7.93 (dd, 2 H, J = 5.6 Hz), 7.73 (s, 2 H), 7.45 (m, 6 H), 7.37 (s, 2 H), 3.60 (t, 4 H, J = 6.0 Hz), 1.76 (q, 4 H, J = 6.0 Hz), 1.4 (s, 18 H). ^{13}C NMR (400 MHz, DMSO-d_6): δ 173.3, 150.3, 143.1, 140.0, 139.7, 133.5, 131.9, 128.3, 125.4, 120.4, 117.2, 104.7, 101.0, 97.5, 85.2, 67.8, 36.0, 30.1, 26.0. ESIMS (DMSO): found *m*/*z* 771.2, calcd *m*/*z* 771.2 for [M − THF + DMSO + H^+]. Anal. Calcd for $C_{42}H_{36}N_4O_2Zn \cdot C_4H_8O$: C, 72.10; H, 5.79; N, 7.31. Found: C, 72.36; H, 5.69; N, 7.03.

1,2-Diaminobenzene-*N,N′*-bis(3-*tert*-butyl-5-(3′-ethynylpyridyl)-salicylidene)zinc(II)·THF (Zn-8). This compound was isolated as an orange solid (98%). ^{1}H NMR (DMSO-d_6): δ 9.08 (s, 2 H), 8.69 (s, 2 H), 8.52 (s, 2 H), 7.92 (m, 4 H), 7.68 (s, 2 H), 7.43 (bs, 4 H), 7.35 (s, 2 H), 3.51 (s, 4 H, overlapped with water peak), 1.75 (bs, 4 H), 1.48 (s, 18 H). The ^{13}C NMR data could not be obtained due to the low solubility of **Zn-8** in common deuterated organic solvents. ESIMS (DMSO): found *m*/*z* 771.2, calcd *m*/*z* 771.2 for [M − THF + DMSO + H^+]. Anal. Calcd for $C_{42}H_{36}N_4O_2Zn \cdot THF$: C, 72.10; H, 5.79; N, 7.31. Found: C, 72.16; H, 5.89; N, 7.07.

General Procedure for the Synthesis of Loop Complexes 9−11. In a 10-mL round-bottom flask equipped with a magnetic stirbar and a water-cooled reflux condenser, *cis*-$(PEt_3)_2Pt(OTf)_2$ (0.05 mmol), the appropriate Schiff base ligand (0.05 mmol), and CD_3NO_2 (2 mL) were combined, heated to 50 °C for 1 h, and then allowed to cool to room temperature. Subsequently, the product was precipitated out by adding excess cold ether and the solid was isolated by filtration.

[*cis*-$(PEt_3)_2Pt(\mu$-1**$)]_2(OTf)_4$ (9).** This compound was isolated as an orange solid (99%). ^{1}H NMR (400 MHz, CD_3NO_2): δ 14.7 (s, 4 H), 8.84 (d, 4 H, J = 4.8 Hz), 8.79 (s, 4 H), 7.96 (d, 4 H, J = 6.4 Hz), 7.91 (d, 4 H, J = 2.0 Hz), 7.85 (d, 4 H, J = 1.6 Hz), 7.49 (m, 4 H), 7.43 (m, 4 H), 2.01 (m, 24 H), 1.44 (s, 36 H), 1.34 (m, 36 H). ^{31}P-{^{1}H}NMR (162 MHz, CD_3NO_2): δ 0.62 (s, J_{Pt-P} = 3056 Hz). ^{19}F NMR (377 MHz, CD_3NO_2): δ −80.1 (s). ESIMS: found *m*/*z* = 1162.5, calcd *m*/*z* 1162.4 for [(M − 2OTf)$^{2+}$]. Anal. Calcd for $C_{104}H_{136}F_{12}N_8O_{16}P_4Pt_2S_4$: C, 47.59; H, 5.22; N, 4.27. Found: C, 47.65; H, 5.17; N, 4.07. Single crystals of **9** suitable for X-ray crystallography were grown by slow diffusion of ether vapor into a concentrated CH_3NO_2 solution of **9**.

[*cis*-$(PEt_3)_2Pt(\mu$-2**$)]_2(OTf)_4$ (10).** This compound was isolated as a yellow solid (98%). ^{1}H NMR (400 MHz, CD_3NO_2): δ 15.7 (s, 4 H), 8.81 (d, 4 H, J = 4.8 Hz), 8.58 (d, 4 H, J = 2.4 Hz), 8.90 (d, 4 H, J = 6.4 Hz), 7.79 (d, 4 H, J = 1.6 Hz), 7.65 (s, 4 H), 2.00 (m, 24 H), 1.50 (s, 24 H), 1.33 (m, 36 H), 1.18 (s, 36 H). ^{31}P{^{1}H} NMR (162 MHz, CD_3NO_2): δ 0.66 (s, J_{Pt-P} = 3076 Hz). ^{19}F NMR (377 MHz, CD_3NO_2): δ −80.1 (s). ESIMS: found *m*/*z* 731.1, calcd *m*/*z* 731.0 for [(M − 3OTf)$^{3+}$]. Anal. Calcd for $C_{104}H_{152}F_{12}N_8O_{16}P_4Pt_2S_4 \cdot CH_3NO_2$: C, 46.68; H, 5.78; N, 4.67. Found: C, 46.60; H, 6.08; N, 4.76. Single crystals of **10**·$2CH_3NO_2$ suitable for X-ray crystallography were grown by slow diffusion of ether vapor into a concentrated CH_3NO_2 solution of **10**.

[*cis*-$(PEt_3)_2Pt(\mu$-7**$)]_2(OTf)_4$ (11).** This compound was isolated as a red solid (96%). ^{1}H NMR (400 MHz, DMSO-d_6): δ 14.8 (s, 4 H), 9.04 (bs, 8 H), 8.95 (s, 4 H), 7.78 (bs, 10 H), 7.52 (bs, 12 H), 1.81 (m, 24 H), 1.36 (s, 36 H), 1.20 (t, 36 H, J = 8.0 Hz). ^{31}P{^{1}H} NMR (162 MHz, DMSO-d_6): δ 4.8 (s, J_{Pt-P} = 3114 Hz). ^{19}F NMR (377 MHz, CD_3NO_2): δ −78.3 (s). ESIMS: found *m*/*z* 757.6, calcd *m*/*z* 757.6 for [(M − 3OTf)$^{3+}$]. Anal. Calcd for $C_{112}H_{136}F_{12}N_8O_{16}P_4Pt_2S_4 \cdot CH_2Cl_2$: C, 48.35; H, 4.96; N, 3.99. Found: C, 48.00; H, 4.68; N, 3.85. Single crystals of **11** suitable for X-ray crystallography were grown by slow diffusion of ether vapor into a concentrated CD_3NO_2 solution of **11**.

General Procedure for the Synthesis of Square Complexes 12−15. Method A. In a 10-mL round-bottom flask equipped with a magnetic stirbar and a water-cooled reflux condenser, *cis*-$(PEt_3)_2Pt(OTf)_2$ (0.05 mmol), the appropriate Zn(II)-metalated ligand (0.05 mmol), THF (2 drops), and acetone (4 mL) were combined and heated to 50 °C for 6 h, during which time much of the desired product precipitated. Additional product was precipitated by adding excess cold ether and was isolated by filtration.

Method B. In a drybox, Et_2Zn (0.05 mmol) was added via a gastight syringe to a 10-mL round-bottom flask equipped with a magnetic stirbar and contained a THF/acetone (2 drops/4 mL) solution of the appropriate loop complex (0.05 mmol). The resulting mixture was stirred at room temperature overnight. Excess cold ether was added, and the resulting precipitate was isolated by filtration.

Method C. In a drybox, Et_2Zn (0.05 mmol) was added via a gastight syringe to a 10-mL round-bottom flask equipped with a magnetic stirbar and contained a CH_3CN (4 mL) solution of the appropriate loop complex (0.05 mmol). The resulting mixture was stirred at room temperature overnight. Excess cold ether was added, and the resulting precipitate was isolated by filtration.

[*cis*-$(PEt_3)_2Pt(\mu$-Zn-1**$)]_4(OTf)_8$ (12).** This compound was prepared via both methods A and B, and is a yellow solid (87%). ^{1}H NMR (400 MHz, acetone-d_6): δ 9.32 (s, 8 H), 9.09 (bs, 16 H), 8.19 (s, 8 H), 8.04

(bs, 24 H), 7.81 (s, 8 H), 7.46 (s, 8 H), 2.01 (m, 48 H), 1.46 (s, 72 H), 1.36 (m, 72 H). $^{31}P\{^1H\}$ NMR (162 MHz, acetone-d_6): δ 0.62 (s, J_{Pt-P} = 3069 Hz). ^{19}F NMR (377 MHz, acetone-d_6): δ −79.2 (s). ESIMS (CH_3CN): found m/z = 959.5, calcd m/z 959.7 for [(M + CH_3CN − 5OTf)$^{5+}$]. Anal. Calcd for $C_{208}H_{264}F_{24}N_{16}O_{32}P_8Pt_4S_8Zn_4$·4THF: C, 46.46; H, 5.15; N, 3.87. Found: C, 46.66; H, 5.20; N, 3.69.

[*cis*-(PEt$_3$)$_2$Pt(μ-Zn-2)]$_4$(OTf)$_8$ (13). This compound was prepared via all three methods A, B, and C, and is a yellow solid (88%). ^1H NMR (400 MHz, acetone-d_6): δ 8.98 (d, 16 H, J = 5.6 Hz), 8.68 (s, 8 H), 7.96 (s, 8 H), 7.93 (d, 16 H, J = 6.4 Hz), 7.69 (s, 8 H), 3.40 (s, 16 H), 2.09−1.99 (m, 48 H), 1.43−1.20 (m, 192 H). $^{31}P\{^1H\}$ NMR (162 MHz, acetone-d_6): δ 0.52 (s, J_{Pt-P} = 3068 Hz). ^{19}F NMR (377 MHz, acetone-d_6): δ −79.2 (s). ESIMS: found m/z 771.9, calcd m/z 771.9 for [(M − 6OTf)$^{6+}$]. Anal. Calcd for $C_{208}H_{296}F_{24}N_{16}O_{32}P_8Pt_4S_8$-$Zn_4$·4THF: C, 46.20; H, 5.68; N, 3.85. Found: C, 46.34; H, 5.81; N, 4.14.

[*cis*-(PEt$_3$)$_2$Pt(μ-Zn-3)]$_4$(OTf)$_8$ (14). This compound was prepared via method A in CH_3NO_2/THF mixture and is a yellow solid (90%). ^1H NMR (400 MHz, CD_3CN): δ 8.64 (d, 8 H, J = 4.8 Hz), 8.59 (d, 8 H, J = 5.6 Hz), 8.48 (s, 8 H), 7.86 (d, 8 H, J = 6.4 Hz), 7.83 (d, 8 H, J = 6.4 Hz), 7.80 (s, 8 H), 7.72 (s, 8 H), 3.36 (s, 8 H), 2.32−1.92 (m, 80 H), 1.54 (s, 72 H), 1.39−1.33 (m, 72 H). $^{31}P\{^1H\}$NMR (162 MHz, CD_3CN): δ 0.68 (s, J_{Pt-P} = 3086 Hz). ^{19}F NMR (377 MHz, CD_3CN): δ −77.3 (s). ESIMS: found m/z 771.9, calcd m/z 771.8 for [(M − 6OTf)$^{6+}$]; found m/z = 541.6, calcd m/z 541.7 for [(M − 8OTf)$^{8+}$]. Anal. Calcd for $C_{208}H_{288}F_{24}N_{16}O_{32}P_8Pt_4S_8Zn_4$·4THF: C, 46.27; H, 5.55; N, 3.85. Found: C, 46.06; H, 5.69; N, 3.97.

[*cis*-(PEt$_3$)$_2$Pt(μ-Zn-7)]$_4$(OTf)$_8$ (15). This compound was prepared via all three methods A, B, and C, and is an orange solid (92%). ^1H NMR (400 MHz, acetone-d_6): δ 9.13 (bs, 8 H), 9.06 (d, 8 H, J = 4.0 Hz), 8.93 (s, 8 H), 7.82 (dd, 8 H, J = 5.6 Hz), 7.63 (d, 8 H, J = 2.0 Hz), 7.56 (d, 8 H, J = 6.8 Hz), 7.42 (m, 16 H), 7.36 (d, 8 H, J = 2.0 Hz), 3.81 (s, 8 H), 2.14−2.06 (m, 48 H), 1.46−1.29 (m, 144 H). $^{31}P\{^1H\}$ NMR (162 MHz, acetone-d_6): δ 0.33 (s, J_{Pt-P} = 3069 Hz). ^{19}F NMR (377 MHz, acetone-d_6): δ −79.3 (s). ESIMS: found m/z 1399.5, calcd m/z 1399.9 for [(M + 5THF + H − 3OTf)$^{4+}$]. Anal. Calcd for $C_{224}H_{264}F_{24}N_{16}O_{32}P_8Pt_4S_8Zn_4$·THF: C, 47.49; H, 4.75; N, 3.89. Found: C, 47.66; H, 4.54; N, 3.68.

[*cis*-(PEt$_3$)$_2$Pt(μ-4)]$_2$(OTf)$_4$ (16). This compound was prepared from ligand **4** and *cis*-(PEt$_3$)$_2$Pt(OTf)$_2$ using essentially the same procedure as that for the preparation of loop complexes **9**−**11**. Complex **16** is a yellow solid (95%). ^1H NMR spectroscopy of the isolated product indicates that it comprises a mixture of two species in equilibrium in solution. ^1H NMR (400 MHz, CD_3NO_2): δ 14.6 (s), 14.5 (s), 9.13 (s), 9.04 (s), 8.69 (m), 8.78 (d, J = 4.8 Hz), 8.21 (d, J = 8.0 Hz), 8.17 (d, J = 8.4 Hz), 7.74 (t, J = 6.0 Hz), 7.67 (t, J = 6.0 Hz), 7.59 (d, J = 1.2 Hz), 7.57 (s), 7.41 (m), 7.37 (s), 7.31 (s), 2.05 (m), 1.48−1.33 (m), 1.29 (s), 1.27 (s). $^{31}P\{^1H\}$ NMR (162 MHz, CD_3NO_2): δ 0.74 (s, J_{Pt-P} = 3098 Hz). ^{19}F NMR (377 MHz, CD_3NO_2): δ −79.8 (s). ESIMS: found m/z = 1312.2, calcd m/z 1312.4 for [MH$^+$] based on a monometallic structure; found m/z 1162.4, calcd m/z 1162.3 for [(M − OTf)$^+$] based on a monometallic structure; found m/z 872.1, calcd m/z 872.1 for [(M − 3OTf + H)$^{4+}$] based on a trimetallic structure. Anal. Calcd for $C_{104}H_{136}F_{12}N_8O_{16}P_4Pt_2S_4$: C, 47.59; H, 5.22; N, 4.27. Found: C, 47.42; H, 5.03; N, 4.26. Single crystals of **16** suitable for X-ray crystallography were grown by slow diffusion of ether vapor into concentrated CD_3NO_2 solution of **16**.

[*cis*-(PEt$_3$)$_2$Pt(μ-Zn-4)]$_2$(OTf)$_4$ (17). In the drybox, Et_2Zn (4.8 mg, 0.039 mmol) was added to a 10-mL round-bottom flask equipped with a magnetic stirbar and contained a solution of **16** (50 mg, 0.019 mmol) in CH_3CN (4 mL). The resulting mixture was stirred at room temperature overnight. Excess cold ether was added and the orange precipitate was isolated by filtration (51 mg, 94%). ^1H NMR (400 MHz, DMSO-d_6): δ 9.21 (s, 4 H), 8.86 (s, 4 H), 8.44 (d, 4 H, J = 4.0 Hz), 8.01 (d, 4 H, J = 7.2 Hz), 7.97 (s, 4 H), 7.78 (s, 4 H), 7.57 (s, 4 H), 7.44 (m, 8 H), 2.50 (m, 24 H), 1.55 (s, 36 H), 1.09 (m, 36 H). $^{31}P\{^1H\}$ NMR (162 MHz, DMSO-d_6): δ 0.52 (s, J_{Pt-P} = 3098 Hz). ^{19}F NMR (377 MHz, CD_3NO_2): δ −78.3 (s). ESIMS: found m/z 1401.1, calcd m/z 1401.9 for [(M + 5CH_3CN − OTf + H)$^{2+}$]. Anal. Calcd for $C_{104}H_{132}F_{12}N_8O_{16}P_4Pt_2S_4Zn_2$·THF: C, 45.94; H, 5.00; N, 3.97. Found: C, 45.99; H, 5.36; N, 3.68.

[*cis*-(PEt$_3$)$_2$Pt(μ-4-CrCl)]$_2$(OTf)$_4$ (18). In the drybox, solid $CrCl_2$ (12 mg, 0.098 mmol) was added to a 10-mL round-bottom flask equipped with a magnetic stirbar and contained a solution of **16** (129 mg, 0.049 mmol based on a dinuclear structure) in THF (20 mL). The mixture was stirred for 3 h under N_2, then opened to the air and stirred for an additional 3 h. The solution was then reduced in volume to ~5 mL under reduced pressure. Subsequently, cold ether (100 mL) was added to precipitate a reddish brown solid. The solid was collected on a frit and dried in air to afford **18** (126 mg, 92%). ESIMS: found m/z 819.4, calcd m/z 819.9 for [(M − Cl − 2OTf)$^{3+}$]. Anal. Calcd for $C_{104}H_{132}Cl_2Cr_2F_{12}N_8O_{16}P_4Pt_2S_4$: C, 44.69; H, 4.76; N, 4.01. Found: C, 44.42; H, 4.91; N, 3.75.

X-ray Crystallography. Crystals of **7**, **9**, **10**, **11**, and **16** were mounted on a glass fiber using oil. All measurements were made on a Brüker SMART-1000 CCD area detector equipped with graphite monochromated Mo Kα radiation. The structures were solved by direct methods[17a] and expanded using Fourier techniques.[17b] The non-hydrogen atoms were refined anisotropically. The SQUEEZE technique was used to refine some solvent as diffused contribution without specific atom positions.[18] Hydrogen atoms were included in idealized positions, but not refined. All calculations were performed using the Brüker SHELX-TL crystallographic software package.[19] Experimental and crystallographic parameters for **7**, **10**, **11**, and **16** are collected in Tables 1 and 2.

Table 1. Crystallographic Data for **7**·CH_2Cl_2 and **10**·2CH_3NO_2

	7·CH_2Cl_2	**10**·2CH_3NO_2
chemical formula	$C_{43}H_{40}Cl_2N_4O_2$	$C_{106}H_{158}F_{12}N_{10}O_{20}P_4Pt_2S_4$
fw, g/mol	715.69	2762.73
temp, K	153 (2)	293 (2)
wavelength, Å	0.710 73	0.710 73
crystal system	monoclinic	monoclinic
space group	$C2/c$	$P2_1/n$
a, Å	18.020 (4)	11.323 (3)
b, Å	22.933 (5)	21.521 (9)
c, Å	9.7801 (14)	26.931 (10)
α, deg		90
β, deg	108.509 (11)	91.53 (3)
γ, deg		90
V, Å^3	3832.7 (13)	6560 (4)
Z	4	1
ρ(calcd), g/cm^3	1.240	1.399
μ, mm^{-1}	0.211	2.322
GOF on F^2	1.038	1.098
R1($I > 2\sigma I$)[a]	0.0542	0.0877
wR2[b]	0.1468	0.2265

[a] $R1 = \sum||F_0| - |F_c||/\sum|F_0|$. [b] $wR2 = [\sum(w(F_0^2 - F_c^2)^2/\sum w(F_0^2)^2]^{1/2}$.

Computer Modeling. The initial molecular models were generated by MM2 force field implemented in the CAChe 5.0 program package.[20] Dynamics calculations were then performed for 1000 ps at 300 K. The lowest energy conformer was then subjected to optimization with the MM2 force field.

(17) (a)Sheldrick, G. M. *SHELXS97, Program for Crystal Structure Solution*; University of Göttingen: Göttingen, Germany, 1997. (b) Sheldrick, G. M. *SHELXL97, Program for Crystal Structure Solution*; University of Göttingen: Göttingen, Germany, 1997.
(18) Van der Sluis, P.; Spek, A. L. *Acta Crystallogr., Sect. A* **1990**, *A46*, 194−201.
(19) *Shelxtl for WindowsNT: Crystal Structure Analysis Package*; Brüker: 1997.
(20) *CAChe 5.0 for Macintosh*; CAChe Group, Fujitsu America Inc.: Beaverton, OR, 2001.

Chart 1

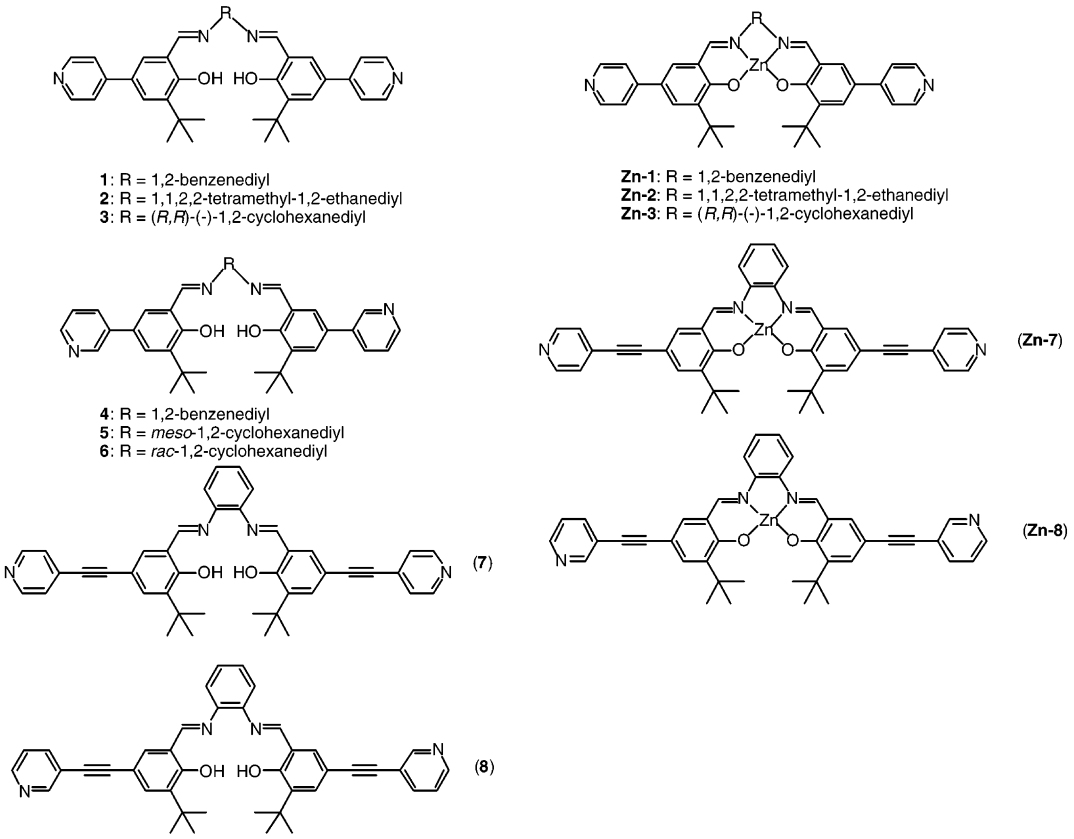

Table 2. Crystallographic Data for **11**·$2CH_3NO_2$ and **16b**·$2CH_3NO_2$

	11·$2CH_3NO_2$	**16b**·$2CH_3NO_2$
chemical formula	$C_{110}H_{126}F_6N_8O_{12}P_4Pt_2S_2$	$C_{104.5}H_{122}F_{10.5}N_{9.5}O_{19}P_4Pt_2S_{3.5}$
fw, g/mol	2444.36	2640.89
temp, K	153 (2)	153 (2)
wavelength, Å	0.710 73	0.710 73
crystal system	triclinic	triclinic
space group	$P\bar{1}$	$P\bar{1}$
a, Å	14.0905 (15)	13.163 (2)
b, Å	18.562 (2)	22.472 (4)
c, Å	20.621 (2)	24.798 (4)
α, deg	81.740 (2)	94.923 (3)
β, deg	79.988 (2)	101.500 (2)
γ, deg	85.836 (2)	93.843 (3)
V, Å^3	7134.7 (19)	7134.7 (19)
Z	1	2
ρ(calcd), g/cm^3	0.773	1.263
μ, mm^{-1}	1.419	2.123
GOF on F^2	1.005	0.900
R1 ($I > 2\sigma I$)[a]	0.1064	0.0739
WR2[b]	0.2788	0.1803

[a] $R1 = \sum||F_0| - |F_c||/\sum|F_0|$. [b] $wR2 = [\sum(w(F_0^2 - F_c^2)^2/\sum w(F_0^2)^2]^{1/2}$.

Results and Discussion

Synthesis of Bis(pyridyl)-Functionalized Salen Ligands and Their Zn(II) Complexes. Chart 1 summarizes the bis(pyridyl)-functionalized salen ligands used in this study. While salen ligands **1**−**3** were synthesized following literature procedure,[5] the syntheses of salen ligands **4**−**8** required the appropriately functionalized salicylaldehyde which can be prepared using either Suzuki[21] or Sonogashira couplings.[22] Subsequent condensation of these salicylaldehydes and several diamines in refluxing ethanol (Scheme 1) afforded the bis(pyridyl)-functionalized salen ligands **4**−**8** in moderate to good yield (34−88%).

Zinc salen complexes **Zn-1**−**Zn-3** were prepared from the corresponding ligands and Et_2Zn via our published Zn-metalation method.[6] Complexes **Zn-7** and **Zn-8** were also synthesized following a similar procedure by adding Et_2Zn to a stirred THF solution of free-base salen ligands **7** or **8** (Scheme 1). The resulting products were easily purified in essentially quantitative yield by filtration and washing with small amounts of cold THF to remove any unmetalated salen ligand.

Single crystals of ligand **7** were obtained by slow evaporation from a CH_2Cl_2/hexane mixture, and the structure of **7** was determined via X-ray crystallography. An ORTEP representation of **7**·CH_2Cl_2 is shown in Figure 1a. Selected bond lengths and bond angles are listed in Table 3 and are in the range of typical values. The C(11)−C(12) and N(1)−C(4) distances are consistent with a localized triple bond and double bond, respectively. The molecule appears to be linear across the two pyridine moieties, although the two hydroxylated phenyl rings slightly deviate from coplanarity (Figure 1b). The bond angles C(13)−C(12)−C(11) (178.35°) and C(12)−C(11)−C(10) (179.03°) depart only slightly from linearity, suggesting that these ligands could be used to construct molecular squares if the ligands remained sufficiently rigid in solution. As shown below, however, this condition is not satisfied, and consequently, supramolecular structures other than squares are generated.

Synthesis of Molecular Loop Complexes. We initially expected to obtain a molecular square complex by combining equimolar amounts of a cis-ditopic acceptor, *cis*-$(PEt_3)_2Pt(OTf)_2$, and the bis(pyridyl)-functionalized salen ligand **1**. This reaction was carried out in deuterated nitromethane to facilitate monitoring by ^1H NMR. The ^{31}P NMR spectrum of the reaction mixture exhibited a singlet with characteristic ^{195}Pt satellites, consistent

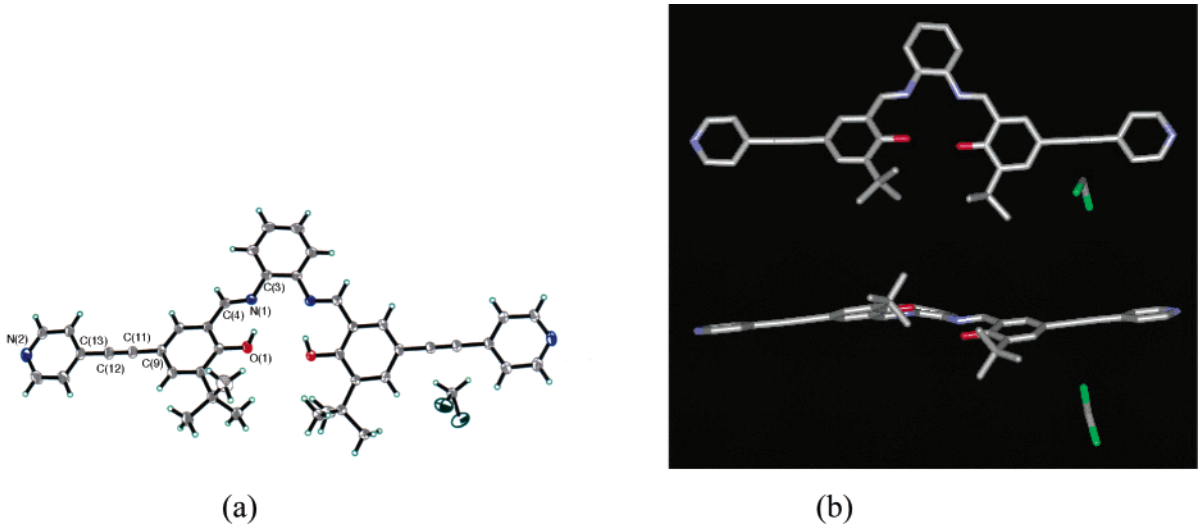

Figure 1. (a) ORTEP diagram of ligand **7** showing atom-labeling scheme and the asymmetric subunit. Thermal ellipsoids are drawn at 50% probability level. (b) Crystal structure of **7** from two views.

Scheme 1

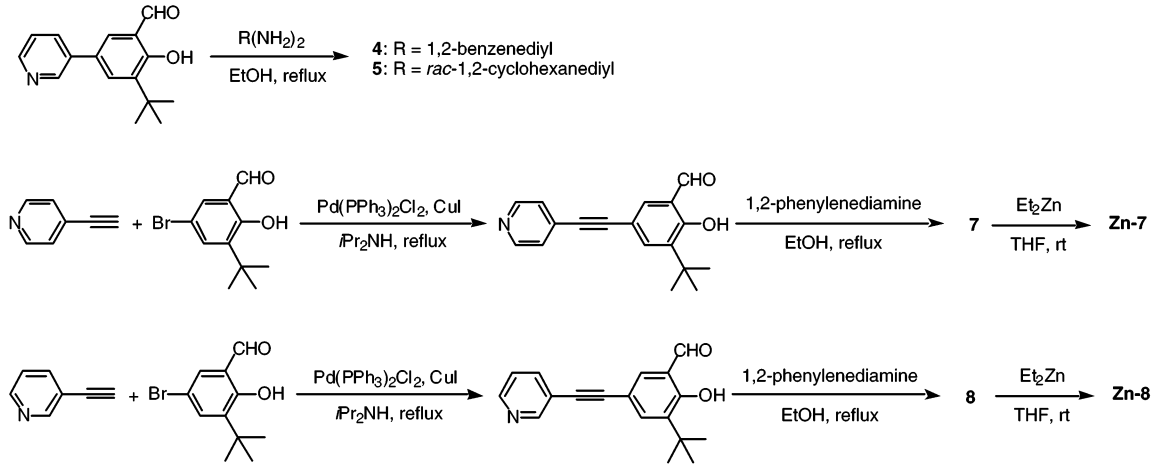

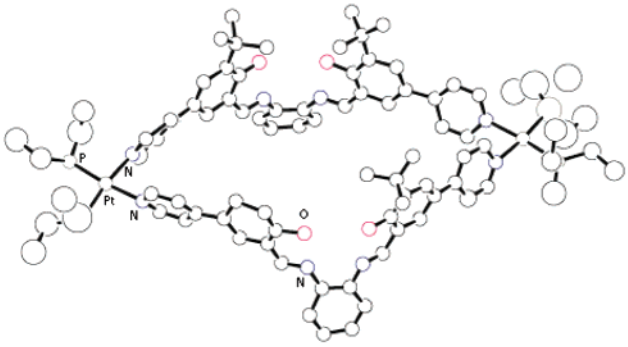

Figure 2. Ball-and-stick representation of loop complex **9**. One *tert*-butyl group, counterions, and solvent molecules are omitted for clarity.

with the presence of a single product. The upfield shift of the ^{31}P signal (~11 ppm) of the directed-assembly product, compared to that of the *cis*-$(PEt_3)_2Pt(OTf)_2$ starting material, is indicative of the coordination of pyridine to the Pt(II) center.[13] The ^{1}H NMR spectrum of the reaction mixture showed only one set of proton signals deriving from ligand **1** and PEt_3. Single crystals of the reaction product were obtained from the diffusion of diethyl ether vapor into the concentrated CD_3NO_2 reaction solution. X-ray diffraction revealed that the product actually has a dinuclear loop structure, rather than the anticipated square structure. Although the quality of the crystal was insufficient to permit a detailed structural analysis, the atom connectivity was unambiguously established (Figure 2). The products from similar reactions between *cis*-$(PEt_3)_2Pt(OTf)_2$ and either ligand **2** or **7** were also crystallographically shown to be loops, not squares (eq 1). Interestingly, attempts to assemble *cis*-$(PEt_3)_2$-$Pt(OTf)_2$ and ligand **3** to form the corresponding dimeric loop were unsuccessful.

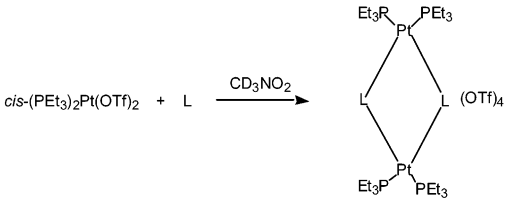

9: L = **1**
10: L = **2**
11: L = **7**

The ORTEP diagram of **10** is shown in Figure 3a, where its shape is almost ellipsoidal. Selected bond lengths and angles are given in Table 4. Loop **10** crystallizes in the monoclinic space group $P2_1/n$ with four cocrystallized CD_3NO_2 solvents. The imine bond distance N(3)−C(32) is short (1.269 (12) Å),

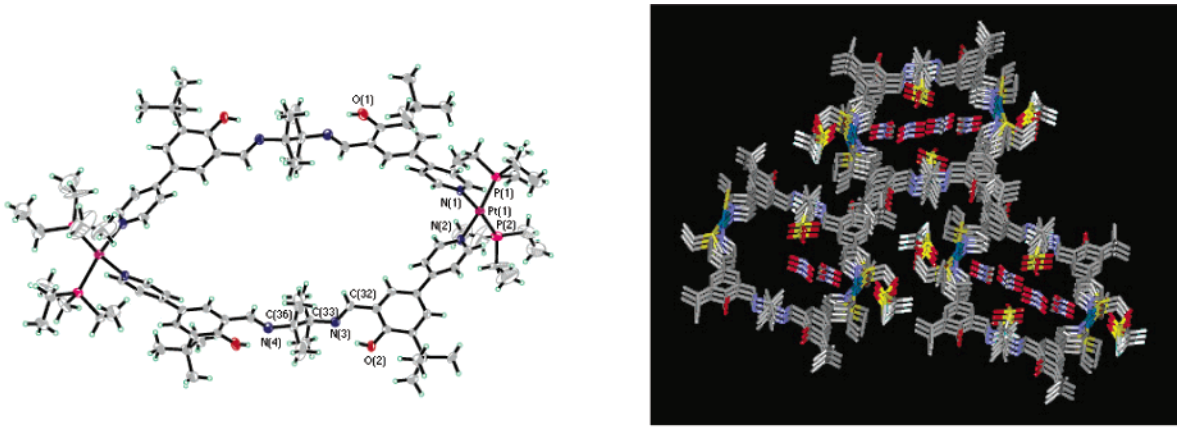

(a) (b)

Figure 3. (a) ORTEP diagram of loop complex **10** showing atom-labeling scheme and the asymmetric subunit. Thermal ellipsoids are shown at 50% probability level. The counterions and solvent molecules are omitted for clarity. (b) Packing diagram with channel formed by the cavity of complex **10** viewed along the *a* axis.

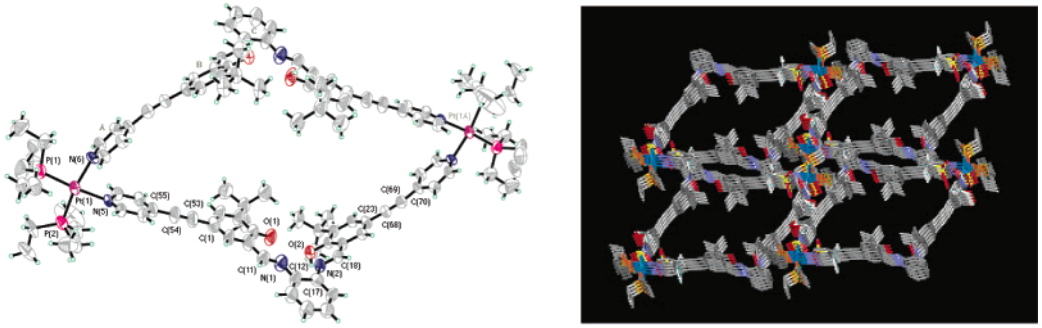

(a) (b)

Figure 4. (a) ORTEP diagram of loop complex **11** showing atom-labeling scheme and the asymmetric subunit. Thermal ellipsoids are shown at 50% probability level. The counterions and solvent molecules are omitted for clarity. (b) Packing diagram with channel formed by the cavity of complex **11** viewed along the *b* axis.

Table 3. Selected Bond Lengths (Å) and Bond Angles (deg) for **7**·CH_2Cl_2

N(1)−C(3)	1.416 (2)	N(1)−C(4)	1.286 (2)
O(1)−C(6)	1.346 (2)	C(9)−C(11)	1.435 (2)
C(11)−C(12)	1.194 (2)	C(7)−C(18)	1.536 (2)
C(4)−N(1)−C(3)	120.52 (12)	N(1)−C(4)−C(5)	122.10 (13)
C(12)−C(11)−C(9)	179.03 (18)	C(11)−C(12)−C(13)	178.35 (19)

Table 4. Selected Bond Lengths (Å) and Bond Angles (deg) for **10**·$2CH_3NO_2$

Pt(1)−N(1)	2.096 (7)	Pt(1)−N(2)	2.121 (7)
Pt(1)−P(1)	2.285 (2)	Pt(1)−P(2)	2.284 (3)
N(3)−C(32)	1.269 (12)	N(3)−C(33)	1.472 (12)
N(1)−Pt(1)−N(2)	84.0 (3)	N(1)−Pt(1)−P(1)	87.1 (2)
N(2)−Pt(1)−P(2)	89.4 (2)	P(1)−Pt(1)−P(2)	99.44 (10)
C(32)−N(3)−C(33)	120.9 (8)		

indicating a localized double bond character. As expected, the pyridine rings of the ligands are not coplanar with adjacent phenyl rings: the dihedral angles are 33.3° and 27.2°. The bridging salen ligands adopt an anti configuration on the diimine backbones, presumably to minimize the strain imposed on the structure. The coordination geometries around the platinum atoms are slightly distorted from ideal 90° angles (N−Pt−N angle = 84.0(2)°) and are similar to those reported for two other cyclic structures containing bis(phosphine) Pt units,[2a,22] where the P−Pt−P angle is widened to 99.4(1)°. The major and minor axes of the loop (Pt−Pt distance and the distance between the centroids of the two salen backbones) are 22.2 and 10.2 Å, respectively.

Table 5. Selected Bond Lengths (Å) and Bond Angles (deg) for **11**·$2CH_3NO_2$

Pt(1)−N(5)	2.127 (6)	Pt(1)−N(6)	2.111 (7)
Pt(1)−P(1)	2.258 (3)	Pt(1)−P(2)	2.281 (3)
C(53)−C(54)	1.186 (16)	C(68)−C(69)	1.186 (14)
N(1)−C(11)	1.253 (15)	N(2)−C(18)	1.279 (12)
N(5)−Pt(1)−N(6)	83.5 (3)	N(6)−Pt(1)−P(1)	91.6 (2)
N(5)−Pt(1)−P(2)	86.65 (19)	P(1)−Pt(1)−P(2)	98.25 (12)
C(53)−C(54)−C(55)	174.6 (17)	C(54)−C(55)−C(1)	179.0 (19)
C(68)−C(69)−C(70)	171.7 (12)	C(69)−C(68)−C(23)	176.4 (11)
C(11)−N(1)−C(12)	124.3 (11)	C(17)−N(2)−C(18)	117.6 (9)

Complex **10** stacks, at a distance of 11.3 Å between Pt centers of adjacent molecules, in such a way as to produce channels along the *a* axis. The channels contain two triflate anions and four CH_3NO_2 solvent molecules per loop molecule (Figure 3b). Similar channel-forming configurations have been observed for related molecular squares and rectangles.[13,14,23c,24]

The ORTEP diagram of **11** is shown in Figure 4a. Selected bond lengths and angles are given in Table 5. Loop complex **11** crystallizes in the triclinic space group $P\bar{1}$ with two cocrystallized CH_3NO_2 solvent molecules. Similar to those of

Scheme 2

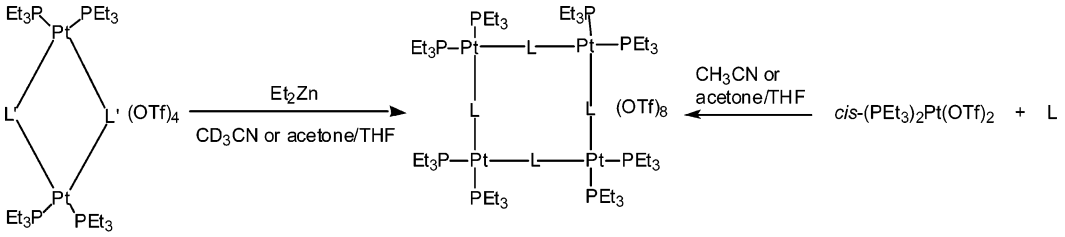

9: L' = **1**
10: L' = **2**
11: L' = **7**

12: L = **Zn-1**
13: L = **Zn-2**
14: L = **Zn-3**
15: L = **Zn-7**

the less-strained loop **10**, the coordination geometries around the platinum atoms are square planar with angles that are slightly distorted from the ideal 90° value (N−Pt−N angles = (83.5-(3)°). The Pt−P and the Pt−N distances are within typical values.[22] The bridging ligand **7** twists in such a way that the molecular shape of **11** is almost rhomboidal. In contrast to **10**, the major strains for **11** are localized between the phenyl rings B and C with a dihedral angle of 37.8°. The C−C≡C−C linkages between the pyridine rings A and phenyl rings B also markedly deviate from linearity. The coordination angles (N−Pt−N angle = 83.5(3)°) are similar to those of the less strained loop **10**. The Pt−Pt distance is 25.4 Å, and the distance between the centroids of the two salen backbones is 15.1 Å. The overall dimensions of the loop, defined by Pt(1)−C(17) and Pt(1A)−C(17) distances, are 15.8 × 13.9 Å.

The packing pattern of **11** is shown in Figure 4b. The cationic loops are stacked along the *b* axis to produce long channels with a distance of 18.6 Å between Pt centers. Two triflate anions were found and refined. They are located directly above and below the P_2-Pt-N_2 plane with Pt−O distances of 3.77 and 4.09 Å, respectively. The other two triflate anions were disordered and not located. Unlike crystals of **10**, whose channels are occupied by counteranions, crystals of **11** feature interlayer packing of counterions, leaving open one-dimensional channels.

Preliminary aqueous electrochemical sieving experiments[10a] with evaporatively cast thin films of loop **11** on Pt electrode surfaces have revealed size selective permeation behavior. For example, smaller redox probes such as ferrocenemethanol (dimensions ∼ 5 × 6 × 6 Å) and $Ru(NH_3)_6^{3+}$ (diameter ∼ 5.5 Å) readily permeate the films while the larger probe, Fe(4,7-bis(*p*-sulfonatophenyl)-1,10-phenanthroline)$_3^{4-}$ (diameter ∼ 24 Å) is completely blocked. These results clearly suggest, but do not prove, that channels derived from molecular cavities are preserved under these conditions.

The preferential formation of bridging-ligand-strained dimetallic loops instead of less strained tetrametallic squares points to the importance of entropy in defining the outcome of the assembly process.[1d,3] The preferential formation of smaller and more strained geometric structures with fewer assembling units over structures with less strain and more assembling units has been reported for several other systems. Sun and Lees, for example, have described the formation of triangles and a loop instead of expected squares or a pseudohexagon when semirigid bridging ligands were combined with $ClRe(CO)_5$.[3b] Kuehl et al. have reported the formation of small rectangles rather than other larger cyclic structures from various flexible ligands and *trans*-$(PEt_3)_2Pt$ corners.[3a]

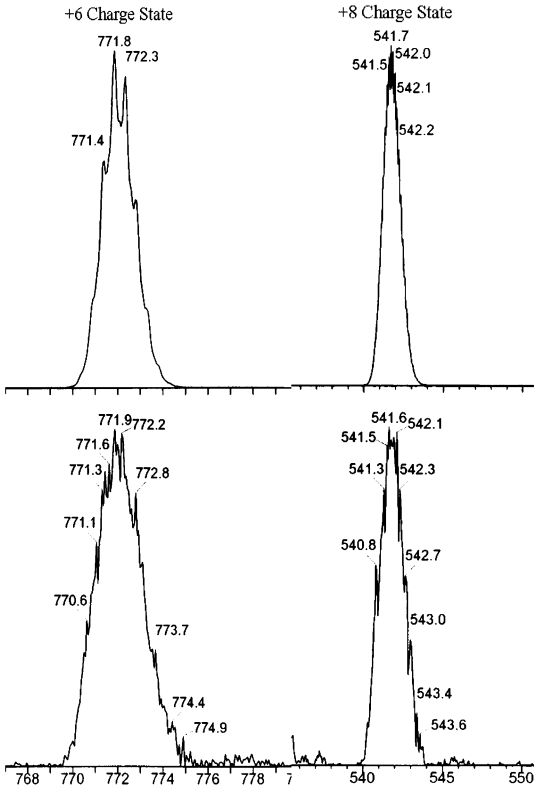

Figure 5. Simulated (top) and experimental (bottom) ESI mass spectra of square **14**.

Assembly of Molecular Squares. We envisioned that Zn(II) metalation of the bis(pyridyl)-functionalized salen ligands would rigidify the ligand framework, thereby precluding loop formation, and at the same time favoring square formation. This is indeed the case (Scheme 2, right-hand side). When equal molar amounts of *cis*-$(PEt_3)_2Pt(OTf)_2$ and a bis(pyridyl)-functionalized Zn(II) salen complex (**Zn-1**, **Zn-2**, **Zn-3**, or **Zn-7**) are mixed in acetone in the presence of a small amount of THF, a single

(21) (a) Suzuki, A. *Pure Appl. Chem.* **1991**, *63*, 419−422. (b) Suzuki, A. *Pure Appl. Chem.* **1994**, *66*, 213−222. (c) Miyaura, N.; Suzuki, A. *Chem. Rev.* **1995**, *95*, 2457−2483. (d) Suzuki, A. *J. Organomet. Chem.* **1999**, *576*, 147−168.
(22) (a) Sonogashira, K.; Tohda, Y.; Hagihara, N. *Tetrahedron Lett.* **1975**, 4467−4470. (b) Takahashi, S.; Kuroyama, Y.; Sonogashira, K.; Hagihara, N. *Synthesis* **1980**, 627−630.
(23) (a) Schweiger, M.; Seidel, S. R.; Arif, A. M.; Stang, P. J. *Angew. Chem., Int. Ed.* **2001**, *40*, 3467−3469. (b) Tabellion, F. M.; Seidel, S. R.; Arif, A. M.; Stang, P. J. *J. Am. Chem. Soc.* **2001**, *123*, 7740−7741. (c) Schmitz, M.; Leininger, S.; Fan, J.; Arif, A. M.; Stang, P. J. *Organometallics* **1999**, *18*, 4817−4824. (d) Habicher, T.; Nierengarten, J.-F.; Gramlich, V.; Diederich, F. *Angew. Chem., Int. Ed.* **1998**, *37*, 1916−1919.
(24) (a) Sun, S.-S.; Anspach, J. A.; Lees, A. J.; Zavalij, P. Y. *Organometallics* **2002**, *21*, 685−693. (b) Slone, R. V.; Hupp, J. T.; Stern, C. L.; Albrecht-Schmitt, T. E. *Inorg. Chem.* **1996**, *35*, 4096−4097.

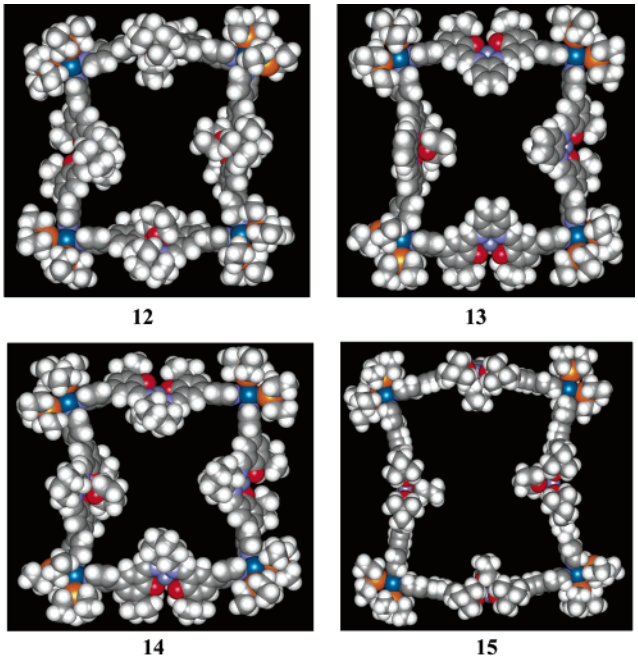

Figure 6. Space-filling models of energy-minimized molecular structures of squares **12**−**15**.

product is formed as evidenced by ^{1}H and ^{31}P NMR spectra. The assignments of products **12**−**15** as squares are made based on ESIMS studies where multiply charged intact molecular ions corresponding to cyclic tetramers were observed. The experimental isotopic distributions for the parent ion of square **14** fit very well with the theoretical calculation (Figure 5). While not without precedent,[25] it is remarkable that these inorganic assemblies would remain intact even at +8 charge state under highly dilute mass spectrometric conditions. Attempts to grow crystals of **12**−**15** suitable for single-crystal X-ray structural evaluation were not successful.

The ^{31}P NMR spectra of squares **12**−**15** all show one singlet with distinct ^{195}Pt satellites. The α and *β* protons of pyridine rings in squares **12** and **13** resonate as broad singlets, but are split into two signals each in squares **14** and **15**. The peak broadening and splitting phenomena are attributed to the restricted rotation of the pyridine rings of the bridging ligands. Similar observations have been reported for other molecular square systems featuring phosphine−Pt(II)−pyridine moieties.[26]

The presence of THF, a coordinating cosolvent, appears to be essential for the assembly of **12**−**15**. Indeed, in the absence of THF (i.e., pure acetone as solvent) only complicated product distributions were obtained. Presumably, THF coordinates axially to Zn(II), thereby preventing aggregation of the bridging moieties (coordination of distal pyridines of one ligand by the electrophilic Zn(II) centers of others).[6]

Notably, the aforementioned complicated mixture of aggregates can be essentially quantitatively converted to the desired square product by adding a few drops of THF and heating at 60 °C for 6 h. These observations underscore the reversible nature of the Pt(II)−pyridine and Zn(II)−pyridine bond formation and the value of the reversibility for subsequent reassembly of desired finite structures (in this case, squares). Not surprisingly, the use of the good coordinating solvent CH_3CN in place of the acetone/THF mixture also works for Scheme 2.

Alternatively, molecular squares **12**, **13**, and **15** can be obtained from the corresponding dimetallic loops (**9**, **10**, and **11**) by Zn metalation of the free-base salen moieties in these loops (Scheme 2, left-hand side). Again, a solvent (CH_3CN or THF) capable of acting as a fifth ligand for Zn(II) is necessary for conversion of the dimetallic loops to the corresponding tetrametallic squares (as opposed to ill-defined aggregate structures).

To the best of our knowledge, these macrocycle expansion processes, driven here by changes in ligand rigidity, represent the first examples of quantitative structural rearrangements involving changes of metal nuclearity in the absence of a template effect.[27] The closest examples are perhaps the observations by Lees and co-workers of interconversions of tetranuclear squares and dinuclear loops via photoinduced ligand isomerization. These conversions were limited, however, by the mixed nature of the ligand photostationary state and, therefore, were not quantitative.[28] Also pertinent are reports by Farrell et al. on the expansion and contraction of rhodium-containing macrocycles via the "weak-link" approach.[29] These reactions, however, do not entail changes of metal nuclearity.[30]

Energy-minimized structures of squares **12**−**15**, based on MM2 molecular modeling,[20] are shown in Figure 6. It is interesting to note that in each case the minimized structure features two distinct bridging ligand conformations: one bowing out from the ideal square configuration and the other bowing in. The sizes of squares **12**−**15**, defined by distances between

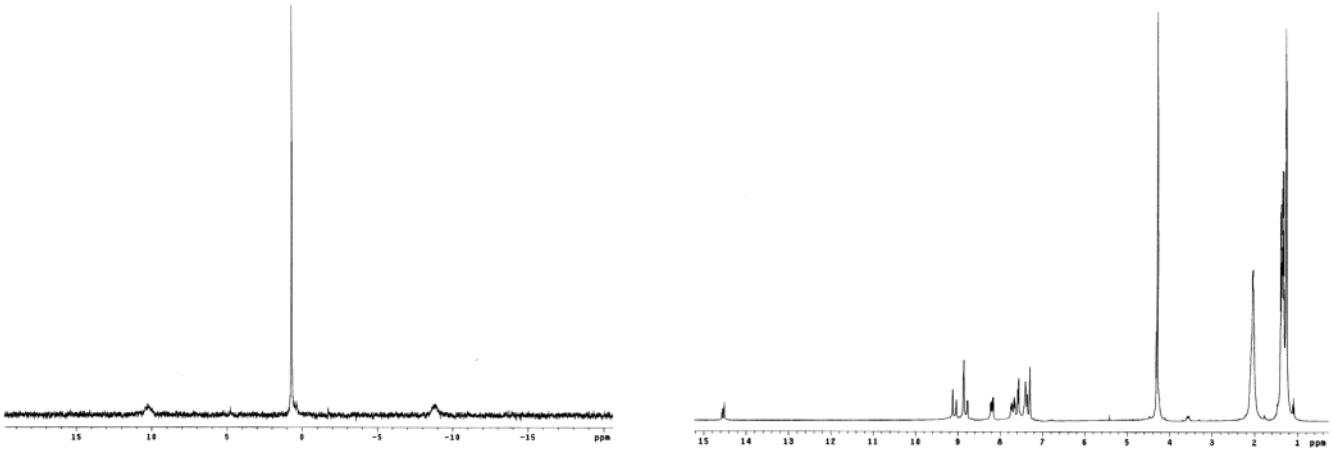

Figure 7. ^{31}P (left) and ^{1}H (right) NMR spectra of solution prepared by combining *cis*-$(PEt_3)_2Pt(OTf)_2$ (40 mM) and ligand **4** (40 mM) in CD_3NO_2.

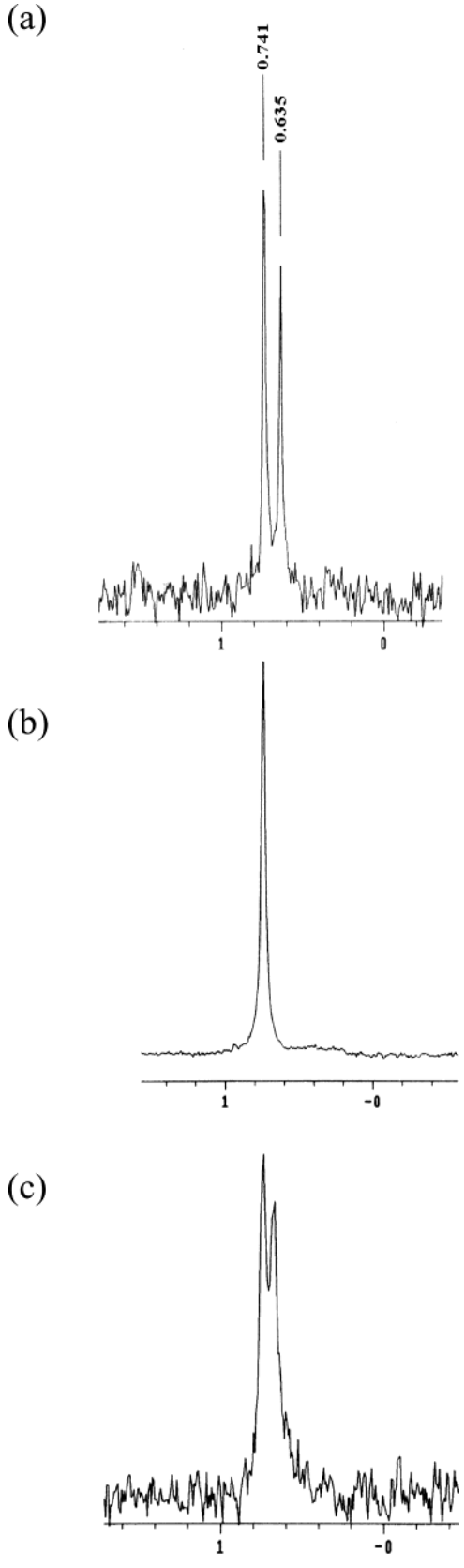

Figure 8. Concentration-dependent ^{31}P NMR spectra of complex **16**: (a) 1-mM solution, (b) 40-mM solution, and (c) 40-mM solution freshly prepared from dinuclear loop crystals.

adjacent platinum corners, are 23.3 × 23.2 Å (**12**), 23.1 × 23.0 Å (**13**), 23.1 × 22.9 Å (**14**), and 28.0 × 27.6 Å (**15**).

Dynamic Equilibria Involving Bis(3-pyridyl)salen-Containing Assemblies. Reconfiguring the functionalized salens as 3-pyridyl rather than 4-pyridyl entities clearly has the potential to yield different assemblies. For example, if the ligands are rigidified by Zn(II) complexation, the linear Pt−N/N−Pt configuration (suitable for square formation) would be replaced by a nonlinear configuration potentially suitable for loop formation. Less predictable is the outcome with flexible, 3-pyridyl-functionalized free-base salens. The experimental finding, detailed below, is that multiple species are formed and exist in concentration-dependent dynamic equilibria.

Suspension of an equal molar amount of the bis(3-pyridyl)-salen ligand **4** in a 40-mM solution of *cis*-$(PEt_3)_2Pt(OTf)_2$ in CD_3NO_2, followed by heating at 70 °C, resulted in ligand dissolution in about 1 h. The ^{31}P NMR spectrum of this reaction mixture showed a single phosphorus peak at 0.74 ppm with characteristic ^{195}Pt satellites (Figure 7, left), while its ^{1}H NMR spectrum exhibited two groups of proton signals with approximately 1:2 integrated intensity (Figure 7, right). When this solution was diluted to <25 mM, a new peak appeared in the ^{31}P NMR spectrum at 0.64 ppm (Figure 8a,b), while the relative intensities of the observed two groups of proton signals also changed, albeit less extensively than the ^{31}P signal. Single crystals obtained from the slow diffusion of diethyl ether into a 40-mM CD_3NO_2 solution were determined to be dimetallic loops (assembly **16b**). However, in solution only a monometallic species, *cis*-[$(PEt_3)_2Pt(OTf)(\eta^1$-**4**$)$](OTf), and a trimetallic species, [*cis*-$(PEt_3)_2Pt(OTf)(\mu$-**4**$)]_3(OTf)_3$, could be detected by ESIMS. Figure 8c shows the ^{31}P NMR spectrum recorded from a 40-mM solution prepared by dissolving single crystals of the dinuclear loop complex **16b**; again, two peaks were observed.[32] Collapse to a single peak matching the resonance at 0.74 ppm occurred after 2 h.

These observations indicate that (a) the major species initially formed from concentrated reactant solution is not the loop

(25) (a) Olenyuk, B.; Whiteford, J. A.; Fechtenkotter, A.; Stang, P. J. *Nature* **1999**, *398*, 796−799. (a) Constable, E. C.; Schofield, E. *Chem. Commun.* **1998**, 403−404. (b) Manna, J.; Kuehl, C. J.; Whiteford, J. A.; Stang, P. J.; Muddiman, D. C.; Hofstadler, S. A.; Smith, R. D. *J. Am. Chem. Soc.* **1997**, *119*, 11611−11619. (c) Manna, J.; Whiteford, J. A.; Stang, P. J.; Muddiman, D. C.; Smith, R. D. *J. Am. Chem. Soc.* **1996**, *118*, 8731−8732. (d) Sun, S.-S.; Lees, A. J. *Inorg. Chem*. **2001**, *40*, 3154−3160. (e) Schalley, C. A.; Müller, T.; Linnartz, P.; Witt, M.; Schäfer, M.; Lützen, A. *Chem. Eur. J.* **2002**, *8*, 3538−3551.

(26) (a) Würthner, F.; Sautter, A.; Schmid, D.; Weber, P. J. A. *Chem. Eur. J.* **2001**, *7*, 894−902. (b) Iengo, E.; Milani, B.; Zangrando, E.; Geremia, S.; Alessio, E. *Angew. Chem., Int. Ed.* **2000**, *39*, 1096−1099. (c) Fuss, M.; Siehl, H. U.; Olenyuk, B.; Stang, P. J. *Organometallics* **1999**, *18*, 758−769.

(27) Representative examples of template-induced structural rearrangements involving changes of metal nuclearity: (a) Campos-Fernández, C. S.; Clérac, R.; Koomen, J. M.; Russell, D. H.; Dunbar, K. R. *J. Am. Chem. Soc.* **2001**, *123*, 773−774. (b) Scherer, M.; Caulder, D. L.; Johnson, D. W.; Raymond, K. N. *Angew. Chem., Int. Ed.* **1999**, *38*, 1588−1592. (c) Cho, Y. L.; Uh, H.; Chang, S.-Y.; Chang, H.-Y.; Choi, M.-G.; Shin, I.; Jeong, K.-S. *J. Am. Chem. Soc*. **2001**, *123*, 1258−1259. (d) Albrecht, M.; Blau, O.; Fröhlich, R. *Chem. Eur. J*. **1999**, *5*, 48−56. (e) Hiraoka, S.; Yi, T.; Shiro, M.; Shionoya, M. *J. Am. Chem. Soc.* **2002**, *124*, 14510−14511.

(28) Sun, S.-S.; Anspach, J. A.; Lees, A. J. *Inorg. Chem*. **2002**, *41*, 1862−1869.

(29) (a) Farrell, J. R.; Mirkin, C. A.; Guzei, I. A.; Liable-Sands, L. M.; Rheingold, A. L. *Angew. Chem., Int. Ed.* **1998**, *37*, 465−467. (b) Holliday, B. J.; Farrell, J. R.; Mirkin, C. A.; Lam, K.-C.; Rheingold, A. L. *J. Am. Chem. Soc.* **1999**, *121*, 6316−6317.

(30) Dynamic equilibria (as opposed to complete interconversion) between triangles and squares (see refs 2 and 25e) and loops and triangles (see refs 23c and 31) have been reported.

(31) (a) Fujita, M.; Aoyagi, M.; Ogura, K. *Inorg. Chim. Acta* **1996**, *246*, 53−57. (b) Ma, G.; Jung, Y. S.; Chung, D. S.; Hong, J.-I. *Tetrahedron Lett*. **1999**, *40*, 531−534.

(32) The entire process of dissolving the crystals and acquiring the ^{31}P NMR spectrum took less than 15 min.

Scheme 3

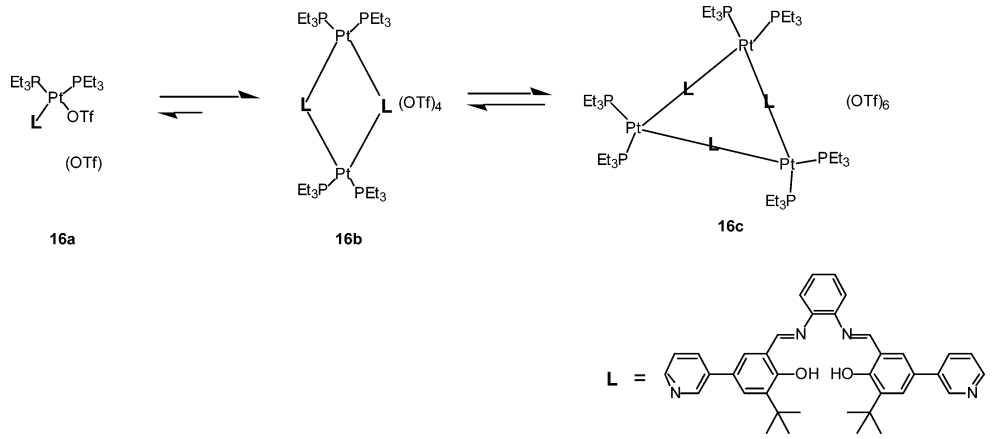

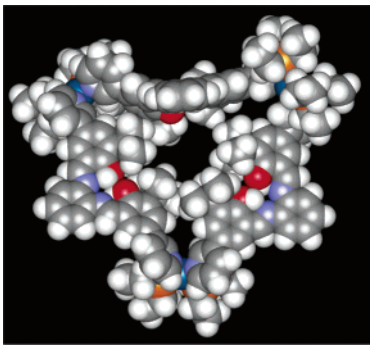

Figure 9. Energy-minimized structure of trimetallic species of **16c** showing two different spatial arrangements of the bridging salen ligands.

assembly, **16b**, but (b) the initially formed assembly exists in dynamic equilibrium with **16b**. One candidate for the dominant initially formed assembly would be a catenated loop pair.[33] The catenated structure can be ruled out, however, as it would generate three groups of proton signals—one corresponding to the free dinuclear structure and two others of equal intensity corresponding to the inside protons and outside protons of the catenate.[33] A more plausible interpretation, especially in view of the ESIMS data, is illustrated in Scheme 3. The species with ^{31}P signal at 0.64 ppm is assigned to the dimetallic loop, a minor product at high concentration. A trimetallic species exists as the major product at higher concentration. The observations of a single phosphorus signal in ^{31}P NMR spectrum but two sets of proton signals in ^{1}H NMR spectrum at high concentration indicate that the bridging salen ligands in the trimetallic species exhibit two different conformations, which do not affect the geometry at the Pt center. As shown in Figure 9, the energy-minimized structure of **16c** after dynamic conformation calculation features two distinct salen ligand conformations, consistent with the NMR spectroscopic findings. On the other hand, under the conditions that the mass spectrometry experiment is carried out, a monomeric compound, **16a**, dominates. The occurrence of multiple equilibria has been well-documented in the literature where flexible ligands were employed in the coordination-driven directed-assembly processes.[2,23c,31] Noteworthy here is that the dominant species in solution (a trinuclear species) is not the species crystallizing from solution (a dinuclear loop). Similar findings have been reported by Stang and co-workers, who found that crystallized square or loop assemblies represented minor solution-phase species.[2a,23c]

Extension of our investigation to other 3-pyridyl-functionalized ligands such as **5**, **6**, and **8** yielded only complicated mixtures upon reaction with *cis*-$(PEt_3)_2Pt(OTf)_2$.[34] This complexity is likely a consequence of the greater flexibility of these ligands in comparison to **4**.

Returning to **4** and the solution-phase mixture of assemblies proposed in Scheme 3, metalation of such a sample with either Zn(II) or Cr(III) yielded samples having clean ^{31}P and ^{1}H NMR spectra characteristic of formation of a single assembly. Figure 10 shows the ^{1}H NMR spectrum of the Zn(II) version of compound **17** in the aromatic region. The disappearance of the characteristic free-base phenol protons around 14.5 ppm and the sharpness of the other peaks point to the formation of a single, highly symmetric Zn(II)-coordinating species. We were unable to obtain crystal structures available for either **17** or **18**. However, ESIMS data unambiguously suggest that both of these products are dimetallic loops (Scheme 4). Similar to the findings described above, quantitative conversion to a single cyclic supramolecular species can be achieved via metalation and rigidification of the salen components of the bridging ligands.[35] Zn(II) and Cr(III) versions of the salen-containing assemblies are of particular interest because of their potential catalytic activity—a point we are exploring in ongoing studies.

Crystal Structures of Bis(3-pyridyl)salen-Containing Assemblies. An ORTEP representation of **16b** is shown in Figure 11. Selected bond lengths and bond angles are collected in Table 6. Perusal of the structure reveals several interesting features. First, no inversion center is observed in the crystal structure of **16b** due to the favorable $\pi-\pi$ stacking interactions of the phenyl rings. The 3-pyridyl coordination directions of ligand **4** allow the aromatic rings in two bridging ligands to align in a way to

(33) (a) Fujita, M.; Ibukuro, F.; Hagihara, H.; Ogura, K. *Nature* **1994**, *367*, 720−723. (b) Fujita, M.; Ibukuro, F.; Yamaguchi, K.; Ogura, K. *J. Am. Chem. Soc.* **1995**, *117*, 4175−4176. (c) Fujita, M. *Acc. Chem. Res.* **1999**, *32*, 53−61.

(34) With ligand **8** as a linker, both monomeric species and dimeric species were observed at *m*/*z* 1210.4, calcd *m*/*z* 1210.4 for $[(M/2 - OTf)^+]$) and *m*/*z* 531.1, calcd *m*/*z* 530.9 for $[(M - 4OTf)^{4+}]$) in the ESIMS spectrum.

(35) Representative examples of template-induced dynamic assembly (not involving rearrangement of existing supramolecular assemblies): (a) Yamanoi, Y.; Sakamoto, Y.; Kusukawa, T.; Fujita, M.; Sakamoto, S.; Yamaguchi, K. *J. Am. Chem. Soc.* **2001**, *123*, 980−981. (b) Ziegler, M.; Miranda, J. J.; Andersen, U. N.; Johnson, D. W.; Leary, J. A.; Raymond, K. N. *Angew. Chem., Int. Ed.* **2001**, *40*, 733−736. (c) Hiraoka, S.; Kubota, Y.; Fujita, M. *Chem. Commun.* **2000**, 1509−1510. (d) Aoyagi, M.; Biradha, K.; Fujita, M. *J. Am. Chem. Soc.* **1999**, *121*, 7457−7458. (e) Hasenknopf, B.; Lehn, J.-M.; Boumediene, N.; Dupont-Gervais, A.; Van Dorsselaer, A.; Kneisel, B.; Fenske, D. *J. Am. Chem. Soc.* **1997**, *119*, 10956−10962. (f) Fujita, M.; Nagao, S.; Ogura, K. *J. Am. Chem. Soc.* **1995**, *117*, 1649. (g) Hiraoka, S.; Fujita, M. *J. Am. Chem. Soc.* **1999**, *121*, 10239−10240.

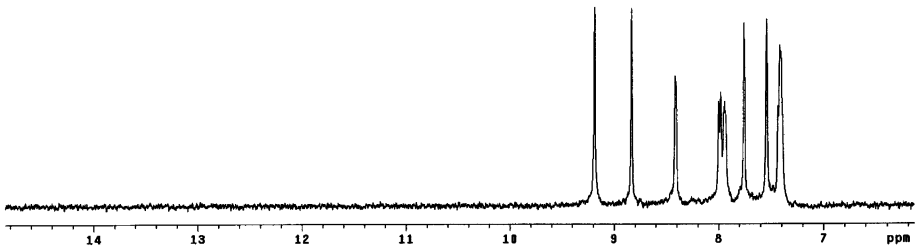

Figure 10. ^{1}H NMR spectrum of **17** in the aromatic region.

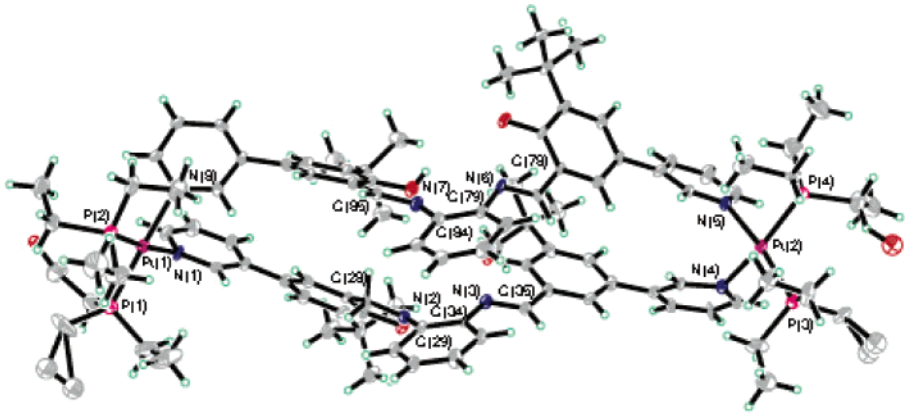

Figure 11. ORTEP diagram of loop complex **16b** showing atom-labeling scheme and the asymmetric subunit. Thermal ellipsoids are shown at 50% probability level. The counterions and solvent molecules are omitted for clarity.

Scheme 4

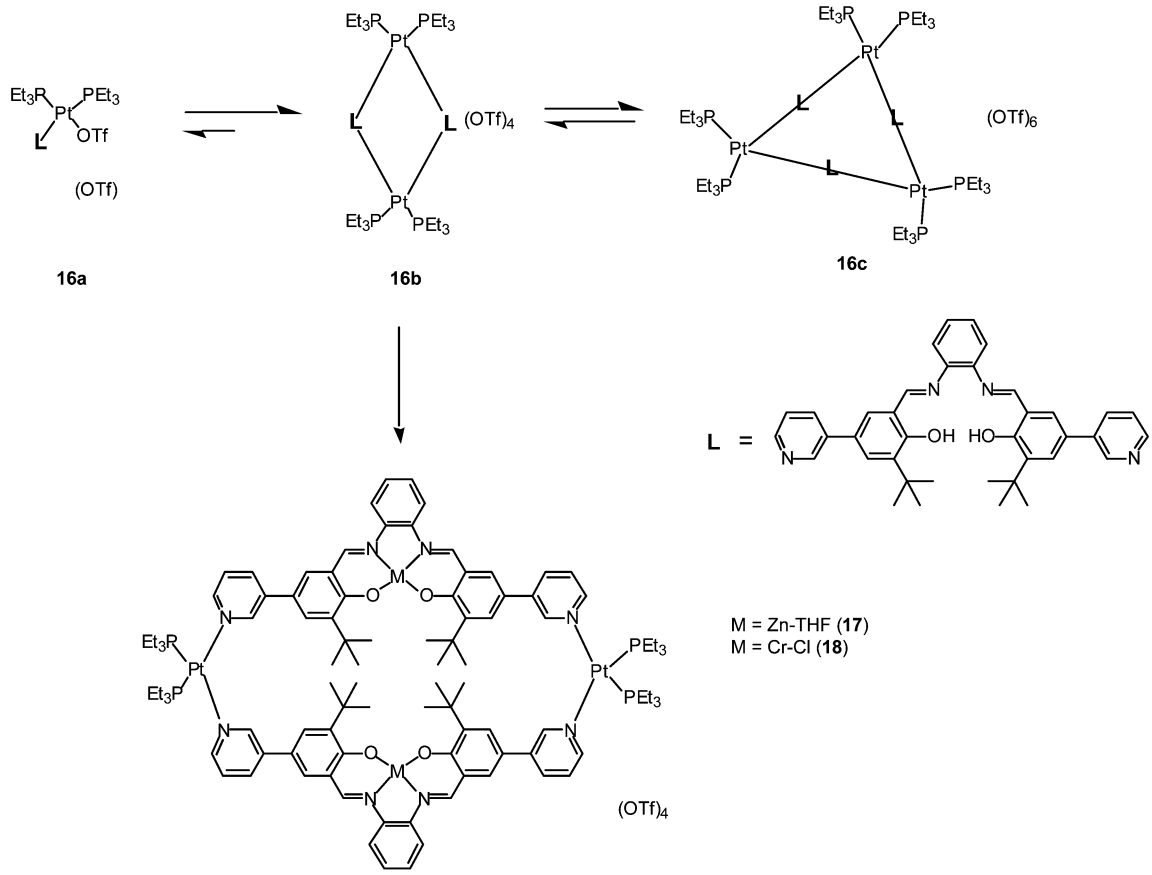

maximize the $\pi-\pi$ interactions. Second, the cavity of the dinuclear loop is small. The distance between the two central phenyl rings is around 3.3 Å and the diagonal Pt−Pt distance is 19.9 Å, leaving no space for guest inclusion as evidenced by no triflate counterions, and solvent molecules occupy inside the cavity. While the average P−Pt−N angle (90.8°) is only slightly

Table 6. Selected Bond Lengths (Å) and Bond Angles (deg) for **16b**·$2CH_3NO_2$

Pt(1)−N(1)	2.127 (7)	Pt(1)−N(8)	2.120 (6)
Pt(2)−N(4)	2.122 (7)	Pt(2)−N(5)	2.101 (7)
Pt(1)−P(1)	2.274 (3)	Pt(1)−P(2)	2.264 (2)
Pt(2)−P(3)	2.270 (2)	Pt(2)−P(4)	2.278 (3)
N(2)−C(28)	1.300 (10)	N(2)−C(29)	1.402 (11)
N(3)−C(35)	1.311 (10)	N(3)−C(34)	1.410 (9)
N(6)−C(78)	1.273 (9)	N(6)−C(79)	1.399 (11)
N(7)−C(85)	1.310 (10)	N(7)−C(84)	1.409 (11)
N(1)−Pt(1)−N(8)	80.9 (3)	N(1)−Pt(1)−P(1)	88.5 (2)
N(8)−Pt(1)−P(2)	92.8 (2)	P(1)−Pt(1)−P(2)	98.04 (9)
N(4)−Pt(2)−N(5)	80.5 (3)	N(4)−Pt(2)−P(3)	92.18 (18)
N(5)−Pt(2)−P(4)	89.9 (2)	P(3)−Pt(2)−P(4)	97.54 (9)
C(28)−N(2)−C(29)	121.8 (7)	C(34)−N(3)−C(35)	119.9 (7)
C(78)−N(6)−C(79)	118.6 (7)	C(84)−N(7)−C(85)	117.8 (7)

deviated from the ideal 90°, the $\pi-\pi$ stacking effect significantly reduces the N−Pt−N angles (average = 80.7°) and enlarges the P−Pt−P angles (average = 97.8°). The platinum−nitrogen bond lengths are similar to those reported for other macrocyclic systems.[23] As expected, the imine nitrogen atoms exhibit a marked sp^2 character with an average C−N−C angle of 119.5° and N=C distance of 1.299 Å. Channels were not found in the crystal structure.

Conclusions

Salen-containing loop structures can be obtained in nearly quantitative yield from *cis*-$(PEt_3)_2Pt(OTf)_2$ and semiflexible difunctional ligands (free-base bis(pyridyl)salens) via a directed-assembly process. Single-crystal X-ray diffraction experiments reveal that the component curvature required for loop closure is achieved via backbone distortion of the bridging salen ligands. The analogous molecular squares can be obtained from loops by linearizing and rigidifying the salen segments of the loops—a process accomplished by complexing Zn(II). Alternatively, squares can be obtained by starting with Zn(II) complexes of bis(4-pyridyl)salens and again combining with *cis*-$(PEt_3)_2Pt(OTf)_2$.

Stoichiometric reaction of a bis(3-pyridyl)salen with *cis*-$(PEt_3)_2Pt(OTf)_2$ produces a mixture of monometallic, dimetallic loop, and trimetallic, likely triangular, species in dynamic equilibrium. High concentrations favor the trimetallic compound, while low concentrations favor the monometallic species. Notably, the species crystallizing from concentrated solutions, which contain predominantly triangular species, is the dimetallic loop. If, prior to reaction with *cis*-$(PEt_3)_2Pt(OTf)_2$, the doubly functionalized salen ligand is rigidified via complexation of Zn(II) or Cr(III), only the dimetallic loop is obtained. The various metalation and concentration-driven interconversions of mono-, di-, tri-, and tetrameric species illustrate the versatile nature of reversible coordination chemistry in the assembly of supramolecular species. The incorporation of metalated salens in several of these species suggests applications in catalytic chemistry, a focus of current studies.

Acknowledgment. We gratefully acknowledge financial support from the NSF and the Northwestern University Institute for Environmental Catalysis. S.T.N. additionally acknowledges support from the duPont Company, the Packard Foundation, and the Sloan Foundation.

Supporting Information Available: Crystallographic data in CIF format, NMR and MS spectra for compounds **12**−**18**. This material is available free of charge via the Internet at http://pubs.acs.org.

JA037378S